

## 5.0 GHz TMRT observations of 71 pulsars

RU-SHUANG ZHAO (赵汝双),<sup>1,2</sup> ZHEN YAN (闫振),<sup>1,3</sup> XIN-JI WU (吴鑫基),<sup>4</sup> ZHI-QIANG SHEN (沈志强),<sup>1,3</sup>  
R. N. MANCHESTER,<sup>5</sup> JIE LIU (刘杰),<sup>1,6</sup> GUO-JUN QIAO (乔国俊),<sup>4</sup> REN-XIN XU (徐仁新),<sup>4</sup> AND KE-JIA LEE (李柯伽)<sup>7</sup>

<sup>1</sup>*Shanghai Astronomical Observatory, Chinese Academy of Sciences  
Shanghai 200030, China*

<sup>2</sup>*University of Chinese Academy of Sciences  
Beijing 100049, China*

<sup>3</sup>*Key Laboratory of Radio Astronomy, Chinese Academy of Sciences  
Nanjing 210008, China*

<sup>4</sup>*School of Physics, Peking University  
Beijing 100871, China*

<sup>5</sup>*CSIRO Astronomy and Space Science  
P.O. Box 76, Epping, NSW 1710, Australia*

<sup>6</sup>*Shanghai Tech University  
Shanghai 201210, China*

<sup>7</sup>*Kavil Institute for Astronomy and Astrophysics, Peking University  
Beijing 100871, China*

(Received; Revised; Accepted)

Submitted to ApJ

### ABSTRACT

We present integrated pulse profiles at 5 GHz for 71 pulsars, including eight millisecond pulsars (MSPs), obtained using the Shanghai Tian Ma Radio Telescope (TMRT). Mean flux densities and pulse widths are measured. For 19 normal pulsars and one MSP, these are the first detections at 5 GHz and for a further 19, including five MSPs, the profiles have a better signal-to-noise ratio than previous observations. Mean flux density spectra between 400 MHz and 9 GHz are presented for 27 pulsars and correlations of power-law spectral index are found with characteristic age, radio pseudo-luminosity and spin-down luminosity. Mode changing was detected in five pulsars. The separation between the main pulse and interpulse is shown to be frequency independent for six pulsars but a frequency dependence of the relative intensity of the main pulse and interpulse is found. The frequency dependence of component separations is investigated for 20 pulsars and three groups are found: in seven cases the separation between the outmost leading and trailing components decreases with frequency, roughly in agreement with radius-to-frequency mapping; in eleven cases the separation is nearly constant; in the remain two cases the separation between the outmost components increases with frequency. We obtain the correlations of pulse widths with pulsar period and estimate the core widths of 23 multi-component profiles and conal widths of 17 multi-component profiles at 5.0 GHz using Gaussian fitting and discuss the width-period relationship at 5 GHz compared with the results at 1.0 GHz and 8.6 GHz.

*Keywords:* pulsars: general, radiation mechanisms: nonthermal

### 1. INTRODUCTION

The mechanism of pulsar radio emission has been a long-outstanding question. A widely accepted theory is that the radio emitting regions are confined to the open polar cap inside the light-cylinder radius (Ruderman & Sutherland

1975). Two different ways can be used to study the pulsar radio emission. Firstly, study of individual pulses at different radio frequencies helps us understand the instantaneous, fluctuating properties of the pulsar emission region (Mitra et al. 2016a). Individual pulse studies reveal a rich set of phenomena such as nulling, mode changing, subpulse drifting and quasi-periodic intensity modulations. Since mode changing was first found in PSR B1237+25 (Backer 1970), dozens of pulsars showing this phenomenon have been revealed. Many of these pulsars exhibit drifting subpulses and nulling (Janssen & van Leeuwen 2004; Redman et al. 2005). Weak emission within the ‘null’ intervals was found in PSR B0826–34, suggesting a mode changing behaviour in this pulsar (Esamdin et al. 2005). Wang et al. (2007) explored the relations between nulling and mode changing for six pulsars in Parkes observations. Simultaneous 328 MHz and 4.85 GHz observations were performed for the subpulse drifting in PSR B0031–07 (Smits et al. 2005). Mode changing properties of PSR B0329+54 were detected in simultaneous 2.3 and 8.6 GHz single-pulse observations (Yan et al. 2018a).

Secondly, integrated profile studies can help us investigate the radio emission geometry and the stable structure and properties of the magnetic field. The profile morphology at different frequencies has been studied for many years (e.g., Rankin 1983a; Lyne & Manchester 1988; Rankin 1992; Mitra & Rankin 2002; Johnston et al. 2008; Hankins & Rankin 2010). Despite the variability of individual pulses, integrated profiles are observed to be highly stable, indicating the global properties of the pulsar magnetosphere. Various morphologies of integrated profiles in different pulsars suggest that the observed variations might be related to different ways of cutting across the radiated beam and the asymmetric and irregular location of the individual pulsar beam components (e.g., Lyne & Manchester 1988; Rankin 1993; Mitra & Deshpande 1999). The frequency dependence of integrated pulse profiles is a key diagnostic of the emission mechanism. Measurements of pulsar flux densities are of great importance for deriving the pulsar luminosity function and investigating the population of radio pulsars at large. Studying the radio spectra of pulsars helps us to understand the emission mechanism (e.g. Lorimer et al. 1995a; Kuniyoshi et al. 2015; Jankowski et al. 2018). In some pulsars at least, the frequency dependence of profile width reflects radius-to-frequency mapping (Cordes 1978) with radio emission at different frequencies at different heights (e.g. Mitra & Rankin 2002). Characteristics of the frequency dependence include: (i) steep intensity spectral index  $\alpha \sim -1.8$  ( $S_\nu \propto \nu^\alpha$ ) (Sieber 1973; Lorimer et al. 1995a) with a range of about 0.0 to  $-4.0$  (Maron et al. 2000), (ii) radio pulsars have a diverse frequency dependence of component separation (Chen & Wang 2014). Many early studies showed that the component separation decreased with increasing frequency but sometimes showed a break between two power laws (e.g. Craft & Comella 1968; Sieber et al. 1975; Rankin 1983a). Mitra & Rankin (2002) studied a sample of 10 pulsars with conal components suggesting three kinds of beam-radius-to-frequency behaviors: a decreasing frequency dependence of pulse width, a decreasing trend but approaching a constant pulse width at higher frequency (cf. Thorsett 1991), and a nearly constant trend of pulse width. (iii) According to the magnetic-pole model, the profile is interpreted as the combination of central core and outer conal emission. The core components of multi-component pulse profiles generally have a steeper spectrum than conal components (Backer 1976; Rankin 1983a; Lyne & Manchester 1988). (iv) The linear polarization level generally decreases with increasing frequency (Manchester et al. 1973; Johnston et al. 2008).

Because of their generally steep radio spectra, pulsars are more difficult to study at higher frequencies, say above a few GHz. Several high-frequency observations have been performed around 5.0 GHz (Seiradakis et al. 1995; Manchester & Johnston 1995; Kijak et al. 1997; von Hoensbroech & Xilouris 1997a; Kijak et al. 1998; Johnston et al. 1998; von Hoensbroech et al. 1998; Kramer et al. 1999). There are 159 pulsars that have been observed in the frequency range from 4 GHz to 5 GHz. The observed profiles of these pulsars provide important information on the emission mechanism. Furthermore, the high-frequency flux densities are important in constraining the spectral behaviour of pulsar radio emission. Some pulsars have a spectral break and some have a spectral peak in the GHz region (Malofeev et al. 1994; Xilouris et al. 1996; Kijak et al. 2011). Thus, the study of pulse intensities and pulse profiles over a wide radio-frequency range (from hundreds of megahertz to tens of gigahertz) is very important for the understanding of the pulsar radiation mechanism and the geometry of pulsar radio emission region.

The Shanghai 65-m Tian Ma Radio Telescope (TMRT) is located at a relatively low latitude and is suited for observing the pulsars located north of  $-45^\circ$  declination. Using the TMRT we have made 5 GHz observations of a sample of 71 pulsars which were expected to be detectable with good signal-to-noise ratio (S/N) at this frequency. A description of the TMRT observations is given in §2. §3 gives the results for individual pulsars. These results are discussed in the context of other observations in §4 and §5 gives a concluding summary.

## 2. OBSERVATIONS

Observations of a sample of 71 pulsars at 5 GHz were performed with the TMRT between 2015 May (MJD 57155) and 2017 December (MJD 58114). The sample was chosen from a list of pulsars with 1.4 GHz flux densities  $\gtrsim 4$  mJy, corresponding to flux densities  $\gtrsim 0.4$  mJy at 5.0 GHz (assuming a spectral index of  $-1.8$ ). Table 1 lists the observational parameters for the 71 pulsars. Initially a central frequency of 5.12 GHz was used, but it was changed to 4.92 GHz and then to 4.82 GHz in late 2015 to avoid radio-frequency interference. The observations were made using the FPGA-based spectrometer digital backend system (DIBAS) (Yan et al. 2015, 2018b) to provide incoherent dedispersion and on-line folding. The total recording bandwidth of 1 GHz was subdivided into 512 frequency channels and each pulsar period was divided into 1024 phase bins. Table 1 lists the total integration time ( $T_{\text{on}}$ ) for each observation. A subintegration time of 30 s was used. Observational data were written out in 8-bit PSRFITS format and PSRCHIVE programs (Hotan et al. 2004) were used for data editing and processing to produce the integrated pulse profiles. Pulsar parameters for on-line folding were obtained from the ATNF Pulsar Catalogue.\*

### 3. RESULTS

Table 1 lists measured flux densities for the 71 observed pulsars, including eight millisecond pulsars (MSPs). For 30 pulsars, the flux densities were calibrated using the calibration sources: 3C48, 3C123, 3C196 or 3C295 (Perley & Butler 2013, 2017). The pulsars calibrated in this way are marked by a \* in Table 1. For the other 41 pulsars which have no real-time flux density calibration, we estimated the mean flux density using the system equivalent flux density (cf., Zhao et al. 2017), which is  $\geq 26$  Jy at 5.0 GHz (Wang et al. 2015). From multiple observations of 3C123 we estimate a 20% calibration uncertainty. This was assumed for pulsars that were observed only once. For pulsars that were observed several times, we selected all observations with S/N higher than 5 and gave the mean flux density and its rms uncertainty in Table 1. For comparison, flux densities around 5 GHz measured by others are listed in the last column in Table 1.

Also listed in Table 1 are  $\Delta\phi(N)$ , where  $\Delta\phi$  is the separation of the outer-most profile components and  $N$  is the number of identifiable components. Pulse widths at 50% and 10% of the profile maximum,  $W_{50}$  and  $W_{10}$  respectively, are also given in Table 1. Component separations and pulse widths were computed from fits of Gaussian profiles to components (cf., Zhao et al. 2017). As for flux densities, for pulsars that were observed several times, mean widths and their uncertainties are given in Table 1.

Mean pulse profiles for the 71 observed pulsars are given in Fig. 1. For 19 pulsars (PSRs J0454+5543, J0738–4042, J0835–4510, J1012+5307, J1509+5531, J1518+4904, J1643–1224, J1713+0747, J1740–3015, J1744–1134, J1745–3040, J1752–2806, J1807–0847, J1829–1751, J1833–0827, J1848–0123, J1935+1616, J1937+2544 and J1955+5059), these profiles have a much better S/N than previous observations at frequencies around 5 GHz (Seiradakis et al. 1995; von Hoensbroech & Xilouris 1997a; von Hoensbroech et al. 1998; Kijak et al. 1998; Johnston et al. 1998; von Hoensbroech 1999; Kramer et al. 1999). For PSRs J0738–4042 and J0835–4510, our profiles with 1024 bins have better time-resolution compared to those with 128 bins in Johnston et al. (1998). The S/Ns of profiles in six pulsars (PSRs J1012+5307, J1509+5531, J1518+4904, J1643–4042, J1744–1134, J1833–0827) are in the range from 10 to 20 in our observations, while in the previous observations, the S/Ns were lower than 10. For PSRs J1745–3040, J1752–2806 and J1848–0123, the profile S/Ns are between 20 to 40 in our observations, which is higher than those in the previous observations. For the rest, in the previous observations, the S/Ns were lower than 33, while in our observations, they are higher than 40. Among the profiles given in Fig. 1, there are 20 where there are no previously published 5 GHz profiles. These, along with other MSPs (PSRs J1012+5307, J1518+4904, J1643–1224, J1713+0747 and J1744–1134) in the sample, are discussed in §3.1 and §3.2 below.

TMRT 5 GHz pulse profiles are compared with profiles at other frequencies obtained from the EPN profile database<sup>†</sup> and ATNF observation database<sup>‡</sup> in Fig. 2. Corresponding components are connected by dashed lines assuming a power-law frequency dependence of component separation as discussed in §4.4. Spectral plots for 27 pulsars are given in Fig. 3 and discussed in §4.1.

#### 3.1. Normal pulsars

In this section we discuss the 19 pulsars for which there are no previously published 5 GHz pulse profiles.

\*<http://www.atnf.csiro.au/research/pulsar/psrcat> (Manchester et al. 2005)

†<http://www.epta.eu.org/epndb>

‡<https://datanet.csiro.au/dap/public/atnf/pulsarSearch.zul>

**PSR J0248+6021.** With 12 years of radio timing data from Nançay Radio Telescope observations, [Theureau et al. \(2011\)](#) published the basic parameters of PSR J0248+6021, which is a relatively young pulsar (characteristic age  $\tau_c \sim 62$  kyr) with a spin period of 217 ms and a large dispersion measure ( $DM = 370$  pc cm<sup>-3</sup>). At 1.4 GHz, profile broadening due to interstellar scattering is evident but at 2.05 GHz and 2.68 GHz the profile has a single narrow component ([Theureau et al. 2011](#)). Fig. 1 shows that at 5.0 GHz there is a single dominant component similar to that at 2.05 GHz and 2.68 GHz, but the profile also has extended wings on either side of this dominant component. These are almost certainly conal emission which has flatter spectrum than the dominant component which can be identified as core emission. The flux density of this pulsar is 3.1 mJy as listed in Table 1 which, within the uncertainties, is consistent with the value of 3.15 mJy obtained by extrapolating with the spectral index of  $-1.19$  given by [Theureau et al. \(2011\)](#).

**PSR J0837-4135 (B0835-41).** This pulsar was discovered at 408 MHz by [Large et al. \(1968\)](#). Published 1400 MHz flux densities ([Taylor et al. 1993](#); [Hobbs et al. 2004](#); [Johnston & Kerr 2018](#)) are variable as are the 5.0 GHz flux densities given in Table 1, suggesting that the observed flux densities are affected by scintillation. However, even with this uncertainty, Fig. 3 suggests a break frequency around 400 MHz. The 5.0 GHz profile for this pulsar (Fig. 1) has a strong central (core) component with two equal outlier (conal) components on each side, similar to that at 8.6 GHz ([Zhao et al. 2017](#)). At 1.4 and 3.1 GHz the central core component completely dominates the profile ([Karastergiou & Johnston 2006](#)), consistent with the normally steeper spectral index for core emission. The separation of the components in longitude is nearly constant with frequency.

**PSR J1559-4438 (B1556-44).** Flux densities of this pulsar at lower frequencies were measured by [Manchester et al. \(1978\)](#), [Fomalont et al. \(1992\)](#) and [Manchester et al. \(1998\)](#). The spectrum from 400 to 5000 MHz shown in Fig. 3 suggests a broken power-law form. The 5 GHz profile has a basically double shape, but with an unresolved asymmetric central component preceding the trailing component by about 3° of longitude. Fig. 2 shows that this offset central component has a much steeper spectrum than the outer components showing that it can be identified as core-type emission despite its offset position. The outer components are clearly conal. These properties are consistent with a gradual change in emission properties across the beam ([Lyne & Manchester 1988](#)) rather than a distinct emission process for core emission ([Rankin 1983a](#)).

**PSR J1651-4246 (B1648-42).** The 5.0 GHz integrated pulse profile given in Fig. 1 has a basically double pulse profile. At lower frequencies, this pulsar has a similar but wider profile, and the components become more equal in amplitude with decreasing frequency ([Johnston & Kerr 2018](#)).

**PSR J1703-3241 (B1700-32).** Observations of this relatively long-period pulsar at frequencies between 0.6 GHz and 1.4 GHz (e.g., [Gould & Lyne 1998](#); [Johnston & Kerr 2018](#)) show that it has a relatively flat-topped profile probably consisting of three overlapping components of similar strength. The 5.0 GHz pulse profile shown in Fig. 1 is consistent with this, perhaps indicating a somewhat weaker and steeper-spectrum central core component. Fig. 3 shows a relatively flat spectrum for this pulsar.

**PSR J1705-3423.** This pulsar was discovered in the Parkes Southern Pulsar Survey by [Manchester et al. \(1996\)](#). It has an approximately gaussian-shaped profile at lower frequencies, perhaps with some structure about the profile peak ([Johnston & Kerr 2018](#)). At 5.0 GHz, the profile (Fig. 1) is more asymmetric with two identifiable components, the leading one about twice the strength of the trailing one. The spectral behaviour is very similar to that of PSR J1703-3241.

**PSR J1707-4053 (B1703-40).** At 1.4 GHz the pulse profile for this relatively high-DM pulsar ( $DM \sim 360$  cm<sup>-3</sup> pc) is dominated by interstellar scattering with no clear intrinsic profile structure ([Johnston & Kerr 2018](#)). At 3.1 GHz, there are two obvious peaks with a relatively weak component at the trailing edge \*. As shown in Fig. 1, at 5.0 GHz, the trailing component is much stronger but the components at the leading part of profile can not be resolved clearly because of the low S/N. The spectrum shown in Fig. 3 has a turn-over around 1.4 GHz.

**PSR J1709-4429 (B1706-44).** This young Vela-like pulsar has been extensively observed at radio frequencies between 450 MHz ([Johnston et al. 1998](#)) and 32 GHz ([Kramer et al. 1997](#)) and has been detected as a  $\gamma$ -ray source with *Fermi* ([Abdo et al. 2013](#)) and *HESS* ([Hoppe et al. 2009](#)). It has a simple highly polarised radio profile with one dominant component (e.g., [Johnston & Kerr 2018](#)). The spectrum is relatively flat as shown in Fig. 3 with a spectral index of  $-0.62$ . Our 5.0 GHz pulse profile (Fig. 1) shows a single component of 50% width about 19° of longitude. This is narrower than the 50% width (20°) at 1.4 GHz ([Johnston & Kerr 2018](#)) and broader than that (16°) at 8.6 GHz ([Zhao et al. 2017](#)).

\*<https://datanet.csiro.au/dap/public/atnf/pulsarSearch.zul>

**PSR J1721–3532 (B1718–35).** This pulsar with a short pulse period of 0.28 s has a very high dispersion measure about  $496 \text{ pc cm}^{-3}$  (Hobbs et al. 2004). At 1.4 GHz the profile is highly scattered (Johnston & Kerr 2018) with a scattering time scale of about 30 ms. At 5.0 GHz, Fig. 1 shows a simple asymmetric profile with a slow rising edge and a steeper falling edge, which is similar to the higher-frequency results from Johnston et al. (2006) and Zhao et al. (2017). Given the flux densities at from 1.4 GHz to 17 GHz, Fig. 3 shows a relatively flat spectrum.

**PSR J1730–3350 (B1727–33).** This pulsar is relatively close both on the sky and in distance to PSR J1721–3532 and is similarly highly scattered at 1.4 GHz (Johnston & Kerr 2018). At 5.0 GHz, Fig. 1 shows that this pulsar has a simple symmetric profile. Fig. 3 suggests that the spectrum is a broken power law which is flatter at high frequencies.

**PSR J1739–2903 (B1736–29).** This pulsar has a relatively strong interpulse separated from the main pulse by very close to  $180^\circ$ . At 0.6 GHz, the ratio of the peak flux of the interpulse to the peak flux of the main pulse is about 42% (Gould & Lyne 1998) and at 1.4 GHz, slightly less, about 40% (Johnston & Kerr 2018). In our observation at 5.0 GHz, the flux density ratio between interpulse and main pulse is about 17%. The longitude separation of the pulse centroid is very close to  $180^\circ$  at all frequencies. Fig. 3 shows a relatively flat spectrum between 400 and 8400 MHz with a spectral index of  $-0.88$ .

**PSR J1809–1917.** This is a young energetic pulsar with pulse period 82.7 ms, age 5.1 kyr and spin-down luminosity  $\sim 1.8 \times 10^{36} \text{ erg s}^{-1}$ . The pulse period is very similar to that of the Vela pulsar, but PSR J1809–1917 is about five times older and five times less energetic than Vela. X-ray observations show that there is an associated pulsar wind nebula (Kargaltsev & Pavlov 2007). At 5.0 GHz, this profile has two widely spaced but overlapping components separated by about  $40^\circ$  of longitude, with the leading component being about half as strong as the trailing one. At 1.4 GHz (Johnston & Kerr 2018), the component separation is larger, about  $54^\circ$ , the components do not overlap and the leading component is a little stronger, about 60% of the trailing one.

**PSR J1835–1106.** This relatively young pulsar ( $\tau_c \sim 100 \text{ kyr}$ ) has a highly polarised symmetric single-component pulse profile at 1.4 GHz (Johnston & Kerr 2018). At lower frequencies, the profile is affected by interstellar scattering (e.g., D’Amico et al. 1998). The 5.0 GHz pulse profile shown in Fig. 1 appears to have some asymmetry. Gaussian fitting shows the profile to have three components with a partially resolved leading component and a weaker trailing one.

**PSR J1844+00** This is a distant, high-dispersion pulsar discovered at 0.4 GHz with a highly scattered profile at that frequency (Camilo et al. 1996). At 1.4 GHz, the scattering is about two orders of magnitude less and the profile is seen to have two components, the trailing one about 30% as strong as the leading one, with a component separation of about  $15^\circ$  (Hobbs et al. 2004). At 5.0 GHz, Fig. 1 shows a similar pulse profile with similar component separation, but with the trailing component a little stronger, about 40% of the leading component. The spectrum of this pulsar has a turn-over around 1 GHz (see Fig. 3).

**PSR J1853+0545.** This middle-aged ( $\sim 3.3 \text{ Myr}$ ) pulsar was discovered at 1.4 GHz in the Parkes Multibeam Survey and shows an apparently scattered profile (observed scattering time about 8 ms or  $24^\circ$  of longitude) at this frequency (Kramer et al. 2003). At 5.0 GHz, Fig. 1 shows that the profile has a dominant leading component with a steep rising edge and a partially resolved trailing component about 30% as strong as the leading component and separated from it by  $\sim 6^\circ$  of longitude. While there are only five measurements of flux density at different frequencies, Fig. 3 suggests that the pulsar has a relatively flat spectral index.

**PSR J1900–2600 (B1857-26).** At low frequencies, this well-known pulsar has a multiple-component profile with a strong central or core component. Five components are distinguished clearly in the profile at frequencies around 300 MHz (Mitra et al. 2016a). The second and central components started merging with each other at 410 MHz and 610 MHz (Gould & Lyne 1998; Mitra et al. 2016a). At frequencies above 1 GHz, all components are merged and have about the same amplitude, giving the profile a flat-topped appearance (e.g., Johnston & Kerr 2018). As Fig. 1 shows, this remains true at 5 GHz. Table 1 shows that the observed 5-GHz flux density is quite stable and Fig. 3 shows that the spectrum between 200 MHz and 5 GHz is a broken power law.

**PSR J1909+1102 (B1907+10).** This pulsar has a relatively short period ( $\sim 0.284 \text{ s}$ ) but a relatively weak magnetic field giving it a characteristic age of about 1.7 Myr. At frequencies lower than 1 GHz, the pulse profile is dominated by a single component. A leading component with peak flux density about 25% of the main component can be seen at 1.4 GHz (Weisberg et al. 1999). Fig. 1 shows that at 5.0 GHz the leading component has a stronger peak flux density than the trailing component. The steeper spectrum of the trailing component is confirmed in Fig. 2 which also shows that the component separation is essentially independent of frequency.

**PSR J2257+5909 (B2255+58).** At low frequencies, below about 1.4 GHz, this pulsar shows two main components with the trailing component dominant (Gould & Lyne 1998). At 1.4 GHz, these two components are of equal strength and there is a hint of a third component trailing the main components by about  $15^\circ$  (Gould & Lyne 1998). Fig. 1 shows that at 5.0 GHz the leading component is the stronger of the two main components. Fig. 2 shows that the separation of these two components is almost constant with frequency. The spectrum shown in Fig. 3 suggests a low-frequency turn-over below about 1 GHz.

**PSR J2330–2005 (B2327-20).** At 410 MHz, three components are visible for this pulsar, with the leading one the strongest and a weak overlapping third component (Gould & Lyne 1998). The observed pulse profile at 5 GHz has rather low S/N (Fig. 1) but within the uncertainties has a similar pulse profile to that at lower frequencies. Fig. 2 shows that the central component becomes somewhat stronger with decreasing frequency, consistent with a core origin. The component separation appears to be independent of frequency. Fig. 3 shows a good fit to a relatively steep power-law spectrum over the frequency range 400 MHz to 5 GHz.

### 3.2. Millisecond pulsars

MSPs form a separate group of pulsars characterised by their short spin period ( $\lesssim 30$  ms) and very low spin-down rate ( $\dot{P} \lesssim 10^{-18}$ ). These properties are attributed to a different evolutionary history involving spin-up, or “recycling”, of an old neutron star by accretion from a binary companion (e.g., Bhattacharya & van den Heuvel 1991). Although implied surface dipole magnetic field strengths are much smaller for MSPs (typically  $10^8 - 10^{10}$  G) compared to normal pulsars ( $10^{11} - 10^{13}$  G), the properties of the observed radio emission, for example, radio spectral indices and polarisation properties, are remarkably similar to those of radio emission from normal pulsars (Kramer et al. 1999; Dai et al. 2015). Although radio luminosities are generally smaller for MSPs, there is a large overlap in the distribution (Kramer et al. 1998). On the other hand, MSP pulse widths are generally much larger, often with significant emission over much of the pulse period, and the spacing of profile components is generally independent of frequency. Observations at high radio frequencies are important in quantifying these trends (Kijak et al. 1997). In our 5 GHz observations, we obtained pulse profiles for eight MSPs (PSRs J1012+5307, J1518+4904, J1600–3053, J1643–1224, PSR J1713+0747, J1744–1134, J1939+2134 and J2145–0750) (Fig. 1). Of these, there is no previous published 5 GHz profile for PSR J1600–3053, for four pulsars (PSRs J1012+5307, J1518+4904, J1643–1224 and J1744–1134) our 5 GHz observations have higher S/N than those in Kramer et al. (1999), and the profile for PSR J1713+0747 at 5 GHz has comparable S/N with the one in Kramer et al. (1999). Descriptions of these six MSPs are given below.

**PSR J1012+5307.** As shown by Kramer et al. (1998), at 1.4 GHz the pulse profile is complex with a broad main pulse having several identifiable components and two interpulses trailing the main peak by about  $110^\circ$  and  $160^\circ$  respectively. Polarisation data at 610 MHz Stairs et al. (1999) show a nearly flat polarization position angle (PA) through all pulse components, suggesting this pulsar might be an aligned rotator.

As shown in Fig. 1, our 5 GHz profile has rather low S/N and only two pulse components can be identified. The observed separation of  $115^\circ \pm 5^\circ$  suggests that we are seeing the trailing components of the main pulse and first interpulse seen at 1.4 GHz. At 5 GHz the interpulse is about 50% as strong as the main pulse, whereas at 1.4 GHz the interpulse is a little weaker, about 40% of the main peak. At 610 MHz it is only about 20% as strong. The separation of these components is the same at all observed frequencies and Fig. 3 shows that, overall, the pulsar has a relatively steep power-law spectrum.

**PSR J1518+4904.** This pulsar has a 40-ms spin period, which is typical of a mildly recycled pulsar. At most frequencies, the pulse profile has two identifiable components spaced by about  $4^\circ$  of longitude with the leading component the stronger of the two (Kramer et al. 1999). However, at 370 MHz there is a weak third component trailing the main component by about  $20^\circ$  (Nice et al. 1996), also seen by Kramer et al. (1998) at 1.4 GHz. Our 5-GHz observation, shown in Fig. 1, which has a S/N comparable to that of the profile shown by Kramer et al. (1999), shows an approximately Gaussian profile of 50% width  $12.5^\circ$  (Table 1). Given the relatively low S/N, it is not possible to distinguish individual components, but the width indicates a blend of the two main components seen at lower frequencies.

**PSR J1600–3053.** The 5-GHz profile shown in Fig. 1 has two identifiable components, spaced by about  $12^\circ$ . In the Parkes three-band observations (Dai et al. 2015), shown in Fig. 2, these two components are clearly seen at 3.1 GHz, but the leading component becomes weaker and more extended with decreasing frequency. This pulsar may be an exception to the general rule that MSP component spacings are independent of frequency. Alternatively, there may be additional blended components at the leading edge of the profile that become stronger at lower frequencies.

**PSR J1643–1224.** This millisecond pulsar is the third most luminous millisecond pulsar after PSRs J0437–4715 and B1937+21. Four components can be identified in the integrated profile at 1.4 GHz (Kramer et al. 1998), with the leading component having a flatter spectrum than the others (Dai et al. 2015). At 5.0 GHz, the leading components is more distinguishable, consistent with this trend.

**PSR J1713+0747.** Parkes observations of this well-known 4.57 ms pulsar at 0.7, 1.4 and 3.1 GHz show at least four components with the third becoming more prominent and narrower with increasing frequency (Dai et al. 2015). The leading component has a relatively flat spectrum, whereas the trailing component has a steeper spectrum (Dai et al. 2015). At 5 GHz, the four components are clearly distinguishable. The component separation is constant with frequency.

**PSR J1744–1134.** At lower frequencies, this isolated MSP has a main pulse consisting of two overlapping components and a double and much weaker precursor pulse leading the main pulse by about  $120^\circ$  (Dai et al. 2015). Fig. 1 shows that at 5.0 GHz there is a partially resolved leading component, consistent with the results of Dai et al. (2015).

## 4. DISCUSSION

### 4.1. Spectra of 27 pulsars

Based on available multi-frequency data between 400 MHz and 9000 MHz, flux-density spectral indices for 27 pulsars are listed in Table 2 along with the pulsar characteristic parameters and references. The corresponding spectra are shown in Fig. 3. For most of the pulsars in our sample, the spectra can be well described by a simple power law ( $S_\nu \propto \nu^\alpha$ ). For seven pulsars, PSRs J0837-4135, J1559–4438, J1707–4053, J1730–3350, J1844+00, J1900-2600, and J2257+5909, the observed spectrum is better fitted by two power laws (cf., Maron et al. 2000; Jankowski et al. 2018), although for three of these, PSRs J0837-4135, J1559-4438 and J1844+00, the interpretation relies on just one discrepant point. Note that for PSR J1730–3350, the spectrum is evidently flatter at high frequencies. Kijak et al. (2017) and Basu et al. (2018) identified PSR J1809–1917 as a “gigahertz-peaked spectrum” pulsar, with a peak flux density around 1 GHz. Basu et al. (2018) fitted the spectrum with a thermal absorption plus power-law model, giving a high-frequency spectral index of  $-1.00^{+0.57}_{-0.98}$ . Jankowski et al. (2018) fitted a power-law spectrum to data between 1 GHz and 7 GHz, obtaining a spectral index of  $-0.4 \pm 0.2$ . **In September 2018 (MJD 58370), we re-observed this pulsar at 2.25 GHz with the total recording bandwidth of 100 MHz for 30 min, to give a calibrated flux density of  $1.1 \pm 0.1$  mJy.** As Fig. 3 shows, we similarly fitted a power law to the high-frequency data and obtained a flatter spectral index of  $-0.11 \pm 0.26$  (Table 2). For PSR J0837–4135, Jankowski et al. (2018) identified the spectrum as broken power-law, with a break frequency around 700 MHz, but the spectrum in Fig. 3 suggests a break frequency around 400 MHz. For PSR J1703–3241, Jankowski et al. (2018) suggested a weak log-parabolic spectrum, but also fitted a power law, giving a spectral index of  $-1.5 \pm 0.2$ . Our data, shown in Fig. 3, supports the power-law interpretation and gave essentially the same spectral index as that obtained by Jankowski et al. (2018).

To study the spectral index correlations we chose the 19 pulsars that have simple power law spectra plus four more that have well-defined power-law spectra above a break (viz., PSRs J0837–4135, J1707–4053, J1900–2600 and J2257+5909). PSR J0248+6021 is excluded since there are just two measurements of flux density. Fig. 4 shows the Spearman rank correlations of radio spectral index  $\alpha$  with pulsar period  $P$ , period derivative  $\dot{P}$ , characteristic age  $\tau$ , the 1400-MHz pseudo-luminosity  $L_{1400} = S_{1400}d^2$ , the surface magnetic field  $B_{\text{surf}}$  and the spin-down luminosity  $\dot{E}$ .<sup>\*</sup> These correlations were also fitted by weighted power laws giving the results shown in Table 4. The correlation coefficients for all pulsars in our sample, normal pulsars and MSPs are listed in Table 3, along with previous results from Jankowski et al. (2018); Han et al. (2016); Lorimer et al. (1995a). Jankowski et al. (2018) observed 441 pulsars, including nine MSPs, at frequencies between 730 MHz and 3100 MHz. **For the 276 pulsars with simple power-law spectra, they obtained Spearman rank correlations of spectral index with various pulsar parameters.** They found very significant correlations with  $\nu$ ,  $B_{\text{LC}}$  and  $\dot{E}$  for normal pulsars, where  $B_{\text{LC}}$  is the magnetic field strength at the light cylinder. Han et al. (2016) obtained Parkes observations at 1.4 GHz for 224 normal pulsars and combined these data with previously published results for 372 pulsars to give a total sample of 572 normal pulsars. They found a weak correlation of spectral index with spin-down luminosity  $\dot{E}$ . Lorimer et al. (1995a) studied a set of 343 pulsars, including 20 MSPs, for correlations between  $\alpha$  and  $P$ ,  $\dot{P}$ ,  $\tau$ ,  $B_{\text{surf}}$ ,  $\dot{E}$  and pulse width. For normal pulsars, they found two significant correlations:  $\alpha$  with  $P$  and  $\alpha$  with  $\tau$ . For MSPs they found a strong positive correlation of spectral index with  $P$ .

<sup>\*</sup>Pulsar parameters are from the ATNF Pulsar Catalogue.

For all pulsars in our sample, we find that the correlations of spectral index with  $\tau$  and  $\dot{E}$  are relatively strong, whereas we find no correlation with  $B_{\text{surf}}$  and only weak correlation with the other parameters. The stronger correlations are in the sense of steeper spectra for old pulsars and flatter spectra for pulsars with high radio luminosity and high  $\dot{E}$ . In contrast to Lorimer et al. (1995a), we find no strong correlation of MSP spectral indices with pulse period. The most consistent correlation across the different samples is the positive correlation with spin-down luminosity  $\dot{E}$  for normal pulsars. MSPs do not show any strong correlations and results from different samples are different but this may be largely due to the small sample sizes.

#### 4.2. Pulsar profiles with mode changing

Mode changing is a phenomenon, first observed by Backer (1970), in which the pulse profile abruptly changes from a given state to another state. Usually there are just two quasi-stable states or modes (e.g., Wang et al. 2007; Rankin 2017), **but in a few pulsars three or more modes are observed, for example, in PSRs J1822-2256, J1946+1805 and J2321+6024 (Wright & Fowler 1981; Deich et al. 1986; Basu & Mitra 2018)**. Mode changing is closely related to pulse nulling, where the observable emission abruptly ceases for some interval and then resumes equally abruptly (e.g., Wang et al. 2007). Both mode changing and nulling evidently result from an abrupt change in the magnetospheric current distribution, leading to a different radiation beam pattern which, in some cases, has little or no emission directed toward us (Kramer et al. 2006; Timokhin 2010). Simultaneous mode changing in the radio and X-ray emission was detected by Hermsen et al. (2013), suggesting a rapid and global magnetospheric state change.

In our 5-GHz observations, mode changes have been detected in five pulsars: PSRs J0332+5434, J0538+2817, J0742-2822, J1825-0935 and J2022+2854. We discuss each in turn.

PSR J0332+5434 (B0329+54) is a bright pulsar which has frequent mode changing and is therefore an ideal candidate for studying mode changing at different frequencies. Lyne (1971) first found that the ratio of the amplitude of the outer components to that of the central component changed simultaneously at 408 MHz. Bartel et al. (1982) found evidence for several different abnormal modes in this pulsar. They found that the mode changing occurred simultaneously at 1.4 and 9.0 GHz, and concluded that abnormal modes lasted from several periods to hours. Suleimanova & Pugachev (2002) showed that the profile shape changes within one pulse period. High-frequency observations (Kramer et al. 1996, 1997) showed that the mode changing was clearly visible at 32 and 43 GHz. Long term observations performed by Chen et al. (2011) found that this pulsar spent 84.9% of the total time in the normal mode, and 15.1% in the abnormal mode. Six 10-hour observing sessions of this pulsar were performed by Białkowski et al. (2018) with LOFAR at 140 MHz, they found that 12.6% of profiles are abnormal-mode profile which was lower than that in Chen et al. (2011). Simultaneous 13cm/3cm observations for this pulsar was performed by Yan et al. (2018a), and 13% of time for PSR J0332+5434 was in the abnormal mode. Besides, bright narrow pulses, whose peak flux densities are 10 times of those of integrated profile, were observed at both frequencies.

Several observations at 5.0 GHz for this pulsar were performed between MJD 57721 and MJD 57887 with total observation time of 180 mins. Sub-integrations of 300 pulse periods were formed to get relatively stable integrated profiles. We found that 12.5% of profiles were in abnormal mode (see Fig. 5), in agreement with the results of Białkowski et al. (2018) and Yan et al. (2018a), but we found no evidence for multiple abnormal modes. **Note that, because of our 300-period sub-integrations, some short bursts of abnormal mode may have been missed.** The left panel of Fig. 5 shows the comparison between the normal and abnormal modes at 5 GHz. In both modes, there are three main components connected by bridges. In the abnormal mode, the leading and trailing components are of larger amplitude relative to the central component and the trailing component appears earlier by about  $1^\circ$  of longitude (cf. Yan et al. 2018a). The right panel in Fig. 5 shows that the ratio of leading and trailing components to the central one ( $R_{12}$  and  $R_{32}$ ) change simultaneously at mode switching. The duration of the abnormal mode is between 3 and 8 min, which is limited by the sub-integration time and observing time in our sample.

PSR J0538+2817 is a young pulsar associated with the supernova remnant Sim 147. In the discovery paper Anderson et al. (1996) found that the pulsar had two emission modes with the trailing component being relatively weaker in Mode B. Observations at 430 MHz and 1.4 GHz showed that the trailing component has a flatter spectrum and that the mode changes are more pronounced at the higher frequency. There are only two TMRT observations for this pulsar, at MJD 58102 and MJD 58114 (see Table 1). Fig. 6 shows that the spectral evolution of the modes continues to higher frequencies, with the trailing component dominating the profile in Mode A at 5 GHz. We also find that the profile components are wider and overlap more in Mode A.



For PSR J0742–2822 (B0740–28), in observations at 1.4 GHz and 3.1 GHz, [Keith et al. \(2013\)](#) found interesting mode change behaviour with complex changes in the pulse profile between two modes which they labelled as Mode I and Mode II. Generally the trailing half of the profile is relatively stronger in Mode II. They also found that Mode II was associated with a higher spindown rate and that this correlation was stronger after a glitch and remained so for about 3 years. In our 5.0 GHz observations, this pulsar was observed on a number of occasions between MJD 57291 to MJD 57887. The left panel in Fig. 7 shows that the mode-changing behaviour at 5.0 GHz is similar to that at lower frequencies although the trailing components in both modes are more prominent at 5.0 GHz. In Mode II, the trailing component is broader, leading to an increased overall pulse width in this mode. Observed mode changes at frequencies around 8 GHz ([Johnston et al. 2006](#); [Zhao et al. 2017](#)) have similar properties. For this pulsar, stable integrated profiles can be obtained by averaging pulses over 1.5 min (about 550 rotation periods). We find that the ratio between leading and trailing components ( $R_{12}$ ) varies frequently between 0.45 to 0.98 at 5.0 GHz. The right panel of Fig. 7 shows the distribution of  $R_{12}$  fitted with two gaussian components following the method of [Wen et al. \(2016\)](#) to distinguish the different modes. Based on these fits, the pulsar is in Mode I for 77% and Mode II for 23% of the total observation time of 4 hours, with durations of Mode I and Mode II in the ranges 10 to 40 minutes and 10 to 20 minutes, respectively.

PSR J1825–0935 (B1822–09) has been observed many times and shown to have complex mode changes and related drifting subpulse behaviour (e.g., [Fowler et al. 1981](#)). In the so-called “quiescent” or Q-mode, the “precursor” component which leads the main pulse by about  $15^\circ$  of longitude is weak and the main component shows strong drifting subpulses. In the “burst” or B-mode, the precursor is much stronger and the drifting behaviour in the main pulse disappears. Even more interestingly, [Gil et al. \(1994\)](#) showed that the interpulse, which is about  $180^\circ$  from the main pulse, becomes relatively much stronger in the Q-mode. This reveals a strong connection between the precursor/main-pulse emission and the interpulse emission which challenges standard orthogonal two-pole models for main-pulse/interpulse structure. [Dyks et al. \(2005\)](#) addressed this issue with a one-pole bi-directional model, in which both the main pulse and the interpulse originate from the same magnetic pole with oppositely directed emission beams forming the precursor and interpulse respectively. [Latham et al. \(2012\)](#) found there was a strong modulation with  $P_3 = 46.6$  rotation periods in Q mode. A weak modulation with 70 rotation periods was found in B mode. They also found a triple structure of the main pulse in both modes and in Q mode that the leading and trailing regions of the main pulse correlated both with each other and with the interpulse. In a 55-hour radio observation [Hermsen et al. \(2017\)](#) found that 63.9% of pulses were in Q mode.

PSR J1825–0935 was observed several times between MJD 57378 and MJD 57825 with a total observation time of about 110 mins. Observed durations of B-mode emission were from 1.5 to 15 mins and for Q-mode the durations were from 4 to 14 mins. The left panel in Fig. 8 shows a comparison of the B-mode and Q-mode integrated profiles at 5 GHz. The behaviour is similar to that at lower frequencies with a strong anti-correlation between the intensities of the precursor and interpulse. The 5 GHz observations show that a feature on the trailing side of the main pulse becomes stronger and more distinct in Q-mode. For each 30 s sub-integration, we measured the S/N of the main pulse, precursor and interpulse as shown in the right panel of Fig. 8. We find that setting an S/N threshold ( $\sim 3$ ) on the precursor emission distinguishes the different modes clearly. This plot also shows that the precursor is anti-correlated with the interpulse as found at lower frequencies.

Mode changing for PSR J2022+2854 was first discovered at 1.4 GHz ([Wen et al. 2016](#)), and consists of a change of relative intensity between the leading and trailing profile components. Two-component gaussian fitting to the profile was used to obtain the ratio of leading component to trailing one ( $R_{12}$ ) confirming that there are two emission modes (normal and abnormal mode). In their 8 hours quasi-continuous observation, only 11% of profiles averaged over 30 seconds are in abnormal mode.

In our 5.0 GHz observations, this pulsar was observed between MJD 57292 and MJD 57844 and the total observation time was about 96 mins. We also averaged profiles over 30 s. The left panel of Fig. 9 shows the two emission modes at 5 GHz. The right panel shows the distribution of  $R_{12}$  with the normal mode having the smaller values and the abnormal mode represented by the small tail at higher  $R_{12}$ . Of the 167 sub-integrations, about 6% are in abnormal mode in our observations, smaller than the 11% observed at 1.4 GHz ([Wen et al. 2016](#)).

**For another five pulsars (PSRs J0358+5413, J0826+2637, J1239+2453, J1946+1805 and J2321+6024), mode changing has been previously reported, but was not detected in our observations. In most cases, the reason for our non-detection of mode changing is that our observations were of short duration compared to the typical time in “normal” mode. For example, for PSR J0358+5413 (PSR B0355+54)**

**Morris et al. (1980)** found one mode change in over 3 hours which lasted about 5% of the total observation time. For PSR J1239+2453 (PSR B1237+25), **Backer (1970)** found typical normal mode durations of several hours. For PSR J1946+1805 (PSR B1944+17), the profile has relatively low S/N in our 15 min observation, so we cannot distinguish the different modes (**Deich et al. 1986; Kloumann & Rankin 2010**). Similarly, in PSR J0826+2637 (PSR B0823+26) (**Sobey et al. 2015**) and PSR J2321+6024 (PSR B2319+60) (**Wright & Fowler 1981**) it is likely that our observations had insufficient sensitivity to detect the emission in the weaker mode.

#### 4.3. Pulsar profiles with interpulse emission

Interpulses have been found in many pulsars and are especially common in young pulsars (**Weltevrede & Johnston 2008**) and millisecond pulsars (**Dai et al. 2015**). Often the interpulse (IP) lies close to  $180^\circ$  from the main pulse (MP) and for this reason interpulses are commonly assumed to originate near the second pole of a dipolar magnetic field with the magnetic axis approximately perpendicular to the rotation axis. For some pulsars the observed position angle variations are consistent with this idea (**Keith et al. 2010**) whereas in others they are not very consistent (e.g., **Everett & Weisberg 2001; Malov & Nikitina 2013**). Often in these latter cases the separation of the MP and IP is less than  $180^\circ$  and there is a bridge of emission between the two components (**Hankins & Fowler 1986**). These and similar observations led to models in which the MP and IP originate from a single magnetic polar region, possibly with the magnetic axis close to alignment with the rotation axis (e.g., **Manchester & Lyne 1977; Hankins & Cordes 1981**), or with bi-directional emission from a single source region (e.g., **Dyks et al. 2005**). It has been suggested, most recently by **Basu et al. (2015)**, that these wide profiles may be related to the precursor or postcursor components that are seen in some pulsars, e.g., PSR B0823+26, as they generally share some properties such as frequency-independent separation from the main pulse and high linear polarisation.

Six pulsars with interpulses (PSRs J0953+0755, J1012+5307, J1705–1906, J1739–2903, J1825–0935 and J1939+2134) are detected in our 5.0 GHz observations (see Fig. 1 and Fig. 10). All data at other frequencies are from ATNF and EPN pulsar databases. The frequency dependence of MP–IP separations for these six pulsars is shown in Fig. 10 along with weighted power-law fits to the data. Absolute values for spectral indices are all less than 0.01 and consistent with zero, i.e., the MP–IP separations are independent of frequency. This is consistent with previous studies (e.g., **Hankins & Fowler 1986**).

For PSRs J1705–1906, J1739–2903 and J1939+2134, the longitude separations between the IP and MP are  $179^\circ \pm 4^\circ$ ,  $182^\circ \pm 1^\circ$  and  $173^\circ \pm 1^\circ$ , respectively. It is likely that a two-pole model is applicable to these three cases (**Stairs et al. 1999; Weltevrede et al. 2007; Keith et al. 2010; Malov & Nikitina 2013**). However, there are complications. **Dai et al. (2015)** show that for PSR J1939+2134 the polarisation position angle variations are inconsistent with the rotating-vector model (RVM) at each pole, and that there is low-level emission between the two components, similar to that observed in the Crab pulsar (**Hankins et al. 2015**). Furthermore, for PSR J1705–1906, there are in-phase modulations of the IP and MP which are difficult to explain in the two-pole model (**Weltevrede et al. 2007**). Similarly, as discussed in §4.2, the emission of MP and IP of Q-mode of PSR J1825–0935 might be from the same pole (**Gil et al. 1994; Dyks et al. 2005; Malov & Nikitina 2013**), even though the separation between the MP and IP is  $174^\circ \pm 3^\circ$ . There is clearly a relationship between the interpulse and precursor in this pulsar (cf. **Basu et al. 2015**) but, as Fig. 8 shows, the trailing edge of the main pulse also participates in the mode change, so the situation is complicated.

The discussion of PSR J1012+5307 in §3.2 shows that this pulsar might be a nearly aligned rotator with a relatively wide beam (**Kramer et al. 1998; Stairs et al. 1999**) having three main components, although only two (with a separation of  $\sim 115^\circ$ ) are visible at 5 GHz. In PSR J0953+0755, the separation between IP and MP is  $156^\circ \pm 7^\circ$  and is basically frequency independent, the inner edges of the MP and IP are flatter than the outer edges and there is a low-level bridge of emission joining them (**Hankins & Fowler 1986**). **Hankins & Cordes (1981)** showed that the polarisation position angle rotates continuously from the MP through the bridge to the IP. These observations all suggest that the emission in pulsars with component separations similar to or greater than that of PSR J0953+0755 may come from a single wide emission cone, possibly close to alignment with the rotation axis (**Manchester & Lyne 1977; Narayan & Vivekanand 1983; Malov & Nikitina 2013**). The pulse emission from this pulsar may be a wide-separation example of the precursor class as suggested by **Basu et al. (2015)**.

Fig. 10b shows us that for two pulsars (PSRs J1739–2903 and J1939+2134), the ratio of the peak flux of the IP to the peak flux of MP decreases with increasing frequency, and this behavior can be described by a simple power law. For PSR J0953+0755, we find that the IP/MP ratio increases with frequency, in agreement with the results of

Hankins & Fowler (1986). Also in the case of PSR J1012+5307, the behavior of IP/MP ratio with frequency is the same as that in PSR J0953+0755, which is consistent with the low-frequency results of Nicastro et al. (1995). For PSRs J1705–1906 and J1825–0935, there appears to be a maximum IP/MP ratio at about 1.5 GHz, with a decreasing power law at higher frequencies and possibly an increasing one at lower frequencies.

#### 4.4. Frequency dependence of profile width

The frequency dependence of pulse width is a very useful tool for studying the geometry and location of radio emission in the pulsar magnetosphere. Previous studies showed that the component separation  $\Delta\phi$  decreases with increasing frequency with a typical power-law index  $\beta \sim -0.25$ , where  $\Delta\phi \sim \nu^\beta$  (Sieber et al. 1975; Manchester & Taylor 1977; Cordes 1978). By studying the pulsar widths at 333 and 618 MHz Mitra et al. (2016a) found that  $\beta \sim -0.19 \pm 0.1$ . But for some pulsars, two power laws with a break frequency separating the high- and low-frequency regimes better describes the frequency dependence of profile width (Rankin 1983b; Slee et al. 1987). Thorsett (1991) analysed this dependency and concluded that a break frequency is not necessary and that a single power law combined with a minimum pulse width can fit the data at all frequencies. Low-frequency observations for 100 radio pulsars with LOFAR were analysed by Pilia et al. (2016). They found a preference for profile widening at low frequencies, as expected for radius-to-frequency mapping (RFM) (e.g., Cordes 1978), but with a wide spread of  $\beta$  values, including about 15% with  $\beta > 0$ . In some cases this apparent broadening at high frequencies resulted from the appearance of new components at the edge of the profile.

From our observations, 20 pulsars with multiple components are selected to study the frequency dependence of pulsar width. Table 1 lists the separations of the outer components,  $\Delta\phi$ , and the number of discernable components for these pulsars. Including data from previous work (Dai et al. 2015; Gould & Lyne 1998; Weisberg et al. 1999; Seiradakis et al. 1995) and dividing the 20 pulsars into three categories: seven with  $\beta < 0$ , eleven with  $\beta \sim 0$  and two with  $\beta > 0$ , parameters from weighted power-law fits to the frequency dependence are listed in Tables 5, 6 and 7, respectively, and plotted in Fig. 11. The pulse profiles at different frequencies are given in Fig. 2, along with the component phase at each frequency based on the derived power-law fits.

For PSR J1740–3015, the multi-frequency profile comparison for this pulsar was excluded in our earlier work (Zhao et al. 2017) because that the components cannot be resolved clearly at lower frequencies. However, the TMRT profiles at three frequencies (2.3, 5.0 and 8.6 GHz) and the Parkes profile at 1.4 GHz shown in Fig. 2 clearly show that there are two components with the trailing one becoming more obvious at higher frequencies.

In the first group, all but one of the frequency index values are between  $-0.26$  and  $-0.11$  (Table 5), similar to previously reported values. The exception is PSR J2354+6155 which has a much steeper dependence, with index  $-0.58$ . Fig. 2 shows that there is little ambiguity about the component identification and consequently that the rapid frequency evolution of component spacing is likely to be real. We find no evidence for a minimum pulse width at higher frequencies (cf. Thorsett 1991)

Pulsars with component separation index  $< 0.075$  (but excluding interpulse pulsars and MSPs) are listed in Table 6. The reason(s) why these pulsars evidently do not have RFM is not understood. Some, e.g., PSR J1825-0935, may be in the precursor group which may have a distinct emission mechanism (Basu et al. 2015).

There are two pulsars, listed in Table 7, where the components evidently increase in separation with increasing frequency. For PSR J1954+2923, there are two prominent profile components. Fig. 2 shows that the Tian Ma 5 GHz profile clearly has a wider component separation compared to the lower-frequency profiles. For PSR J1946+1805, the identification of the different components at different frequencies is less clear. In Fig. 12, we show the results of fitting Gaussian components to the profiles at the four frequencies. At the lowest frequency only three components are needed but at higher frequencies four are required. These results confirm that the separation of the outermost components increases with frequency (see also Fig. 11) contrary to the standard RFM. We also checked on the effect of the observed mode changing at lower frequencies (Kloumann & Rankin 2010) and found that this has no effect on this conclusion. Whether the increasing separation with frequency results from a different magnetospheric configuration, different emission-region location or different viewing angle is not clear.

#### 4.5. Period dependence of pulse widths

The inverse dependence of pulse widths with pulsar period is a well-established phenomenon (Lyne & Manchester 1988; Rankin 1990, 1993). Rankin (1990) found the lower bound for  $W_{50}$  of core components, normalised to a radio frequency of 1 GHz, is  $2^{\circ}45P^{-0.5}$ . Widths of interpulse pulsars where the magnetic axis was believed to be orthogonal

to the rotation axis followed this relation. Wider observed widths are naturally interpreted as pulsars with more aligned magnetic axes, giving a pulse-width relation for core components:

$$W_{50}^{core,1.0} = 2^{\circ}45P^{-1/2}/\sin\alpha_B. \quad (1)$$

where  $\alpha_B$  is the magnetic inclination angle. [Maciesiak & Gil \(2011\)](#) analysed a much larger sample of interpulse pulsars and obtained the relation:

$$W_{50}^{core,1.0} = (2^{\circ}51 \pm 0^{\circ}08)P^{-0.5 \pm 0.02}. \quad (2)$$

[Maciesiak & Gil \(2011\)](#) and [Maciesiak et al. \(2012\)](#) examined the half-power pulse widths,  $W_{50}$ , of a large sample (about 1500) pulsars and showed that a similar lower bound applied. [Mitra et al. \(2016a\)](#) found the lower bound at 618 MHz to be  $2^{\circ}7P^{-0.5}$  for  $W_{50}$  and  $5^{\circ}7P^{-0.5}$  for  $W_{10}$ . [Pilia et al. \(2016\)](#) used the interpulse pulsars in their 150 MHz sample and obtained the relations  $(3^{\circ}5 \pm 0^{\circ}6)P^{-0.5}$  for  $W_{50}$  and  $(10^{\circ} \pm 4^{\circ})P^{-0.5}$  for  $W_{10}$ . [Skrzypczak et al. \(2018\)](#) studied the profile component widths of 123 normal pulsars at 333 and 618 MHz and found that the core and conal component widths versus period had a lower boundary line following the  $P^{-0.5}$  relation.

As in [Zhao et al. \(2017\)](#), we take triple or multiple components pulsars whose core components can be confirmed at 5.0 GHz to establish a relation between the pulsar period and the core widths. We used gaussian fitting to measure half-power widths of core components at 5.0 GHz,  $W_{50}^{core,5.0}$  and these are given in Table 8. Also listed in Table 8 are the core widths at 1.0 GHz of these pulsars taken directly from [Rankin \(1990\)](#), (cf. [Maciesiak & Gil 2011](#)). The average ratio of 5.0 GHz width to 1.0 GHz width for these pulsars is about 0.93, so we adopt a scale factor for the 5.0 GHz intrinsic core widths of  $2^{\circ}29$ :

$$W_{50}^{core,5.0} = 2^{\circ}29P^{-1/2}/\sin\alpha_B. \quad (3)$$

Fig. 13 shows the observed 5 GHz pulse widths,  $W_{50}$  and  $W_{10}$ , as a function of pulse period. As in [Skrzypczak et al. \(2018\)](#), we estimate the lower bound for  $W_{50}$  and  $W_{10}$  using quantile regression with the quantile of 0.1:

$$W_{50} = (2^{\circ}19^{+0^{\circ}.63}_{-0^{\circ}.49})P^{-(0.50 \pm 0.20)} \quad (4)$$

$$W_{10} = (7^{\circ}08^{+1^{\circ}.04}_{-0^{\circ}.91})P^{-(0.32 \pm 0.10)}. \quad (5)$$

For comparison, the estimated relations,  $(2^{\circ}37 \pm 0^{\circ}13)P^{-0.51 \pm 0.07}$  and  $(2^{\circ}16 \pm 0^{\circ}14)P^{-0.49 \pm 0.08}$ , for  $W_{50}$  at 333 and 618 MHz from [Skrzypczak et al. \(2018\)](#) are also shown in Fig. 13, respectively. The lower boundary lines for  $W_{50}$  at different frequencies are very close and follow the  $P^{-0.5}$  relation. For  $W_{10}$ , the lower boundary line is flatter than that for  $W_{50}$  and is in fact essentially identical to the  $P^{-1/3}$  relation obtained by [Lyne & Manchester \(1988\)](#).

Power-law fits to the period dependence of  $W_{50}$  and  $W_{10}$  gave the results:

$$W_{50} = (6^{\circ}04 \pm 0^{\circ}06)P^{-(0.37 \pm 0.11)} \quad (6)$$

$$W_{10} = (13^{\circ}15 \pm 0^{\circ}05)P^{-(0.37 \pm 0.09)}. \quad (7)$$

These fitted lines are shown on Fig. 13. We can see that the relation of  $W_{50}$  versus period ( $P^{-0.37}$ ) is different to the lower bound relation ( $P^{-0.50}$ ) although within the margin of uncertainty, they are consistent. For  $W_{10}$  the lower-bound and fit indices are essentially the same and both close to  $-1/3$ .

Fig. 14 shows the relation between the observed 5.0 GHz core widths  $W_{50}^{core,5.0}$  and conal widths  $W_{50}^{conal,5.0}$  versus period. In the left panel, we show the estimated minimum boundary scaled to 5 GHz given by Equation 3 and the median regression relation:

$$W_{50}^{core,5.0} = (2^{\circ}75^{+1^{\circ}.05}_{-0^{\circ}.75})P^{-(0.50 \pm 0.26)}. \quad (8)$$

Also shown are the minimum width-period relations obtained by [Rankin \(1990\)](#) and [Zhao et al. \(2017\)](#). The right panel shows the conal component widths obtained by the multi-gaussian fitting, as listed in Table 8. The lower bound for  $W_{50}^{conal,5.0}$  is estimated using quantile regression with the quantile of 0.1:

$$W_{50}^{conal,5.0} = (1^{\circ}32^{+0^{\circ}.26}_{-0^{\circ}.23})P^{-(0.60 \pm 0.14)}. \quad (9)$$

Although different samples give somewhat different relations, overall, we find that the lower boundary lines for conal and core component widths are consistent with a  $P^{-0.5}$  relation within the uncertainties.

We then use Equation 3 to compute the magnetic inclination angles  $\alpha_B^{5.0}$  as listed in the third-last column of Table 8. Corresponding  $\alpha_B$  values for 8.6 GHz from Zhao et al. (2017) and 1 GHz from Rankin (1990) are given in the second-last and last columns, respectively. For some pulsars, the estimated inclination angles at different frequencies are similar to each other, but for others they are not. For example, PSR J0454+5543 was classified as triple pulsar at 1.0 GHz (Rankin 1990), but the central component is split into two at higher frequencies (see Fig. 2), which might account for the discrepant  $\alpha_B$  estimates for this pulsar. For some other pulsars (e.g. PSR J1935+1616), the core emission shows bifurcation behaviour at higher frequencies, perhaps related to orthogonal polarization modes (Mitra et al. 2016b), PSR J1644–4559, another case of discrepant  $\alpha_B$  estimates, shows no sign of either bifurcation or orthogonal modes in the core component, even at 8.5 GHz (Johnston et al. 2006). Keith et al. (2010) applied the rotating vector model (Radhakrishnan & Cooke 1969) to fit the MP and IP inclination angles in PSR J1739–2903 ( $\alpha_B \sim 84^\circ$  for MP,  $\sim 96^\circ$  for IP), which are different to the values we obtained (Table 8). PSR J1955+5059 was classified as single core component in Rankin (1990), but may not in fact be a “core” component. Similarly, fitting of polarization position angles at different frequencies (Blaskiewicz et al. 1991; von Hoensbroech & Xilouris 1997b; Mitra & Li 2004; Everett & Weisberg 2001) give different values of  $\alpha_B$  with a large number of possibilities (Mitra & Li 2004; Everett & Weisberg 2001). The different results obtained for  $\alpha_B$  using different methods for a given pulsar illustrates the fact that all of these methods rely on different assumptions, some of which may not be valid. There is no clear and unambiguous way of determining the magnetic inclination in the general case.

## 5. CONCLUSIONS

Integrated pulse profiles of 71 pulsars, including eight MSPs, have been obtained at 5 GHz with the Shanghai Tian Ma Radio Telescope (TMRT). For 20 pulsars these are the first high-frequency observations and for a further 19 pulsars our results have a higher signal-to-noise ratio (S/N) than the previous observations around this frequency. By combining the 5-GHz data with published data at frequencies between 400 MHz and 9 GHz, radio-frequency spectra are derived for 27 pulsars. For most pulsars the spectra are close to power-law, but for seven, a broken power law is indicated. A significant correlation between power-law slope and characteristic age, 1400 MHz pseudo-luminosity and spin-down luminosity is observed. Mode changing at 5.0 GHz was detected in five pulsars. For six pulsars with interpulses (IP), the separation of the IP and main pulse (MP) was shown to frequency independent, but the ratio of IP to MP intensity is frequency dependent. Comparison of 5.0 GHz profiles with those at other frequencies for 20 pulsars shows three distinct behaviours in the profile width. For seven pulsars, the component separation decreases with frequency; there are eleven pulsars with no significant change in separation between 1 GHz and 5 GHz; for the remaining two pulsars, the separation between the outmost components increases with frequency. The inverse dependence of pulse widths with period is shown at 5.0 GHz and the lower bound at high frequency for pulse widths is estimated. The core half-power widths of 23 pulsars and conal half-power widths of 17 pulsars are measured around 5.0 GHz and a modified width-period relation is given for 5.0 GHz data. Magnetic inclination angles estimated from observed pulse widths are often inconsistent with other estimates, showing that care must be taken when estimating the pulsar geometry.

## ACKNOWLEDGEMENTS

This work was supported in part by the National Natural Science Foundation of China (grants U1631122, 11173046, 11403073, 11633007 and 11673002), the strategic Priority Research Program of Chinese Academy of Sciences, Grant No. XDB23010200, the Knowledge Innovation Program of the Chinese Academy of Sciences (Grant No. KJ CX1-YW-18), and the scientific Program of Shanghai Municipality (08DZ1160100)

## REFERENCES

- |   |   |
|---|---|
| Abdo, A. A., Ajello, M., Allafort, A., & et al. 2013,<br>ArXiv:1305.4385, arXiv:1305.4385 | Bailes, M., Johnston, S., Bell, J. F., et al. 1997, ApJ, 481,<br>386        |
| Anderson, S., Cadwell, B. J., Jacoby, B. A., et al. 1996,<br>ApJ, 468, L55                | Bartel, N., Morris, D., Sieber, W., & Hankins, T. H. 1982,<br>ApJ, 258, 776 |
| Backer, D. C. 1970, Nature, 228, 1297   | Basu, R., & Mitra, D. 2018, MNRAS, 476, 1345                                |
| —. 1976, ApJ, 209, 895  | Basu, R., Mitra, D., & Rankin, J. M. 2015, ApJ, 798, 105                    |

- Basu, R., Rožko, K., Kijak, J., & Lewandowski, W. 2018, *MNRAS*, 475, 1469
- Bhattacharya, D., & van den Heuvel, E. P. J. 1991, *Phys. Rep.*, 203, 1
- Białkowski, S., Lewandowski, W., Kijak, J., et al. 2018, *Ap&SS*, 363, 110
- Blaskiewicz, M., Cordes, J. M., & Wasserman, I. 1991, *ApJ*, 370, 643
- Camilo, F., Nice, D. J., Shrauner, J. A., & Taylor, J. H. 1996, *ApJ*, 469, 819
- Chen, J. L., & Wang, H. G. 2014, *ApJS*, 215, 11
- Chen, J. L., Wang, H. G., Wang, N., et al. 2011, *ApJ*, 741, 48
- Cordes, J. M. 1978, *ApJ*, 222, 1006
- Craft, H. D., & Comella, J. M. 1968, *Nature*, 220, 676
- Dai, S., Hobbs, G., Manchester, R. N., et al. 2015, *MNRAS*, 449, 3223
- D’Amico, N., Stappers, B. W., Bailes, M., et al. 1998, *MNRAS*, 297, 28
- Deich, W. T. S., Cordes, J. M., Hankins, T. H., & Rankin, J. M. 1986, *ApJ*, 300, 540
- Dyks, J., Zhang, B., & Gil, J. 2005, *ApJ*, 626, L45
- Esamdin, A., Lyne, A. G., Graham-Smith, F., et al. 2005, *MNRAS*, 356, 59
- Everett, J. E., & Weisberg, J. M. 2001, *ApJ*, 553, 341
- Fomalont, E. B., Goss, W. M., Lyne, A. G., Manchester, R. N., & Justtanont, K. 1992, *MNRAS*, 258, 497
- Fowler, L. A., Wright, G. A. E., & Morris, D. 1981, *A&A*, 93, 54
- Gil, J. A., Jessner, A., Kijak, J., et al. 1994, *A&A*, 282, 45
- Gould, D. M., & Lyne, A. G. 1998, *MNRAS*, 301, 235
- Han, J., Wang, C., Xu, J., & Han, J.-L. 2016, *Res. Astron. Astrophys.*, 16, 159
- Hankins, T. H., & Cordes, J. M. 1981, *ApJ*, 249, 241
- Hankins, T. H., & Fowler, L. A. 1986, *ApJ*, 304, 256
- Hankins, T. H., Jones, G., & Eilek, J. A. 2015, *ApJ*, 802, 130
- Hankins, T. H., & Rankin, J. M. 2010, *AJ*, 139, 168
- Hermesen, W., Hessels, J. W. T., Kuiper, L., et al. 2013, *Science*, 339, 436
- Hermesen, W., Kuiper, L., Hessels, J. W. T., et al. 2017, *MNRAS*, 466, 1688
- Hobbs, G., Lyne, A. G., Kramer, M., Martin, C. E., & Jordan, C. 2004, *MNRAS*, 353, 1311
- Hobbs, G., Faulkner, A., Stairs, I. H., et al. 2004, *MNRAS*, 352, 1439
- Hoppe, S., de Oña-Wilhemí, E., Khélifi, B., et al. 2009, *ArXiv:0906.5574*, *arXiv:0906.5574*
- Hotan, A. W., van Straten, W., & Manchester, R. N. 2004, *PASA*, 21, 302
- Jankowski, F., van Straten, W., Keane, E. F., et al. 2018, *MNRAS*, 473, 4436
- Janssen, G. H., & van Leeuwen, J. 2004, *A&A*, 425, 255
- Johnston, S., Karastergiou, A., Mitra, D., & Gupta, Y. 2008, *MNRAS*, 388, 261
- Johnston, S., Karastergiou, A., & Willett, K. 2006, *MNRAS*, 369, 1916
- Johnston, S., & Kerr, M. 2018, *MNRAS*, 474, 4629
- Johnston, S., Lyne, A. G., Manchester, R. N., et al. 1992, *MNRAS*, 255, 401
- Johnston, S., Nicastro, L., & Koribalski, B. 1998, *MNRAS*, 297, 108
- Karastergiou, A., & Johnston, S. 2006, *MNRAS*, 365, 353
- Karastergiou, A., Johnston, S., & Manchester, R. N. 2005, *MNRAS*, 359, 481
- Kargaltsev, O., & Pavlov, G. G. 2007, *ApJ*, 670, 655
- Keith, M. J., Johnston, S., Levin, L., & Bailes, M. 2011, *MNRAS*, 416, 346
- Keith, M. J., Johnston, S., Weltevrede, P., & Kramer, M. 2010, *MNRAS*, 402, 745
- Keith, M. J., Shannon, R. M., & Johnston, S. 2013, *MNRAS*, 432, 3080
- Kijak, J., Basu, R., Lewandowski, W., Rožko, K., & Dembska, M. 2017, *ApJ*, 840, 108
- Kijak, J., Kramer, M., Wielebinski, R., & Jessner, A. 1997, *A&A*, 318, L63
- . 1998, *A&AS*, 127, 153
- Kijak, J., Lewandowski, W., Maron, O., Gupta, Y., & Jessner, A. 2011, *A&A*, 531, A16
- Kloumann, I. M., & Rankin, J. M. 2010, *MNRAS*, 408, 40
- Kowalińska, M., Kijak, J., Maron, O., & Jessner, A. 2012, in *Astronomical Society of the Pacific Conference Series*, Vol. 466, *Electromagnetic Radiation from Pulsars and Magnetars*, ed. W. Lewandowski, O. Maron, & J. Kijak, 101
- Kramer, M., Lange, C., Lorimer, D. R., et al. 1999, *ApJ*, 526, 957
- Kramer, M., Lyne, A. G., O’Brien, J. T., Jordan, C. A., & Lorimer, D. R. 2006, *Science*, 312, 549
- Kramer, M., Xilouris, K. M., Jessner, A., et al. 1997, *A&A*, 322, 846
- Kramer, M., Xilouris, K. M., Jessner, A., & Wielebinski, R.; Timofeev, M. 1996, *A&A*, 306, 867
- Kramer, M., Xilouris, K. M., Lorimer, D. R., et al. 1998, *ApJ*, 501, 270
- Kramer, M., Bell, J. F., Manchester, R. N., et al. 2003, *MNRAS*, 342, 1299
- Kuniyoshi, M., Verbiest, J. P. W., Lee, K. J., et al. 2015, *MNRAS*, 453, 828

- Large, M. I., Vaughan, A. E., & Wielebinski, R. 1968, *Nature*, 220, 753
- Latham, C., Mitra, D., & Rankin, J. 2012, *MNRAS*, 427, 180
- Levin, L., McLaughlin, M. A., Jones, G., et al. 2016, *ApJ*, 818, 166
- Lorimer, D. R., Yates, J. A., Lyne, A. G., & Gould, D. M. 1995a, *MNRAS*, 273, 411
- Lorimer, D. R., Nicastro, L., Lyne, A. G., et al. 1995b, *ApJ*, 439, 933
- Lyne, A. G. 1971, *MNRAS*, 153, 27P
- Lyne, A. G., & Manchester, R. N. 1988, *MNRAS*, 234, 477
- Lyne, A. G., Manchester, R. N., Lorimer, D. R., et al. 1998, *MNRAS*, 295, 743
- Maciesiak, K., & Gil, J. 2011, *MNRAS*, 417, 1444
- Maciesiak, K., Gil, J., & Melikidze, G. 2012, *MNRAS*, 424, 1762
- Malofeev, V. M., Gil, J. A., Jessner, A., et al. 1994, *A&A*, 285, 201
- Malov, I. F., & Nikitina, E. B. 2013, *Astronomy Reports*, 57, 833
- Manchester, R. N., Han, J. L., & Qiao, G. J. 1998, *MNRAS*, 295, 280
- Manchester, R. N., Hobbs, G. B., Teoh, A., & Hobbs, M. 2005, *AJ*, 129, 1993
- Manchester, R. N., & Johnston, S. 1995, *ApJ*, 441, L65
- Manchester, R. N., & Lyne, A. G. 1977, *MNRAS*, 181, 761
- Manchester, R. N., Lyne, A. G., Taylor, J. H., et al. 1978, *MNRAS*, 185, 409
- Manchester, R. N., & Taylor, J. H. 1977, *Pulsars* (San Francisco: Freeman)
- Manchester, R. N., Taylor, J. H., & Huguenin, G. R. 1973, *ApJ*, 179, L7
- Manchester, R. N., Lyne, A. G., D'Amico, N., et al. 1996, *MNRAS*, 279, 1235
- Manchester, R. N., Hobbs, G., Bailes, M., et al. 2013, *PASA*, 30, 17
- Maron, O., Kijak, J., Kramer, M., & Wielebinski, R. 2000, *A&AS*, 147, 195
- Maron, O., Kijak, J., Kramer, M., & Wielebinski, R. 2000, in *Pulsar Astronomy - 2000 and Beyond*, IAU Colloquium 177, ed. M. Kramer, N. Wex, & R. Wielebinski (San Francisco: Astronomical Society of the Pacific), 227–228
- Mitra, D., Basu, R., Maciesiak, K., et al. 2016a, *ApJ*, 833, 28
- Mitra, D., & Deshpande, A. A. 1999, *A&A*, 346, 906
- Mitra, D., & Li, X. H. 2004, *A&A*, 421, 215
- Mitra, D., Rankin, J., & Arjunwadkar, M. 2016b, *MNRAS*, 460, 3063
- Mitra, D., & Rankin, J. M. 2002, *ApJ*, 322
- Morris, D., Sieber, W., Ferguson, D. C., & N., B. 1980, *A&A*, 84, 260
- Morris, D. J., Hobbs, G., Lyne, A. G., et al. 2002, *MNRAS*, 335, 275
- Murphy, T., Kaplan, D. L., Bell, M. E., et al. 2017, *PASA*, 34, e020
- Narayan, R., & Vivekanand, M. 1983, *ApJ*, 274, 771
- Nicastro, L., Lyne, A. G., Lorimer, D. R., et al. 1995, *MNRAS*, 273, L68
- Nice, D. J., Sayer, R. W., & Taylor, J. H. 1996, *ApJ*, 466, L87
- Perley, R. A., & Butler, B. J. 2013, *ApJS*, 204, 19
- . 2017, *ApJS*, 230, 7
- Pilia, M., Hessels, J. W. T., Stappers, B. W., et al. 2016, *A&A*, 586, A92
- Radhakrishnan, V., & Cooke, D. J. 1969, *Astrophys. Lett.*, 3, 225
- Rankin, J. M. 1983a, *ApJ*, 274, 333
- . 1983b, *ApJ*, 274, 359
- . 1990, *ApJ*, 352, 247
- Rankin, J. M. 1992, in *IAU Colloq. 128: Magnetospheric Structure and Emission Mechanics of Radio Pulsars*, 133
- . 1993, *ApJ*, 405, 285
- Rankin, J. M. 2017, *J. Astrophys. Astr.*, 38, 53
- Redman, S. L., Wright, G. A. E., & Rankin, J. M. 2005, *MNRAS*, 357, 859
- Ruderman, M. A., & Sutherland, P. G. 1975, *ApJ*, 196, 51
- Sayer, R. W., Nice, D. J., & Taylor, J. H. 1997, *ApJ*, 474, 426
- Seiradakis, J. H., Gil, J. A., Graham, D. A., et al. 1995, *A&AS*, 111, 205
- Shang, L.-H., Lu, J.-G., Du, Y.-J., et al. 2017, *MNRAS*, 468, 4389
- Sieber, W. 1973, *A&A*, 28, 237
- Sieber, W., Reinecke, R., & Wielebinski, R. 1975, *A&A*, 38, 169
- Skrzypczak, A., Basu, R., Mitra, D., et al. 2018, *ApJ*, 854, 162
- Slee, O. B., Bobra, A. D., & Alurkar, S. K. 1987, *Aust. J. Phys.*, 40, 557
- Smits, J. M., Mitra, D., & Kuijpers, J. 2005, *A&A*, 440, 683
- Sobey, C., Young, N. J., Hessels, J. W. T., et al. 2015, *MNRAS*, 451, 2493
- Stairs, I. H., Thorsett, S. E., & Camilo, F. 1999, *ApJS*, 123, 627
- Suleimanova, S. A., & Pugachev, V. D. 2002, *Astronomy Reports*, 46, 309
- Taylor, J. H., Manchester, R. N., & Lyne, A. G. 1993, *ApJS*, 88, 529

- Theureau, G., Parent, D., Cognard, I., et al. 2011, *A&A*, 525, A94+
- Thorsett, S. E. 1991, *ApJ*, 377, 263
- Timokhin, A. N. 2010, *MNRAS*, 408, L41
- Toscano, M., Bailes, M., Manchester, R., & Sandhu, J. 1998, *ApJ*, 506, 863
- van Ommen, T. D., D’Alessandro, F. D., Hamilton, P. A., & McCulloch, P. M. 1997, *MNRAS*, 287, 307
- von Hoensbroech, A. 1999, PhD thesis, University of Bonn
- von Hoensbroech, A., Kijak, J., & Krawczyk, A. 1998, *A&A*, 334, 571
- von Hoensbroech, A., & Xilouris, K. M. 1997a, *A&AS*, 126, 121
- . 1997b, *A&A*, 324, 981
- Wang, J. Q., Zhao, R. B., Yu, L. F., et al. 2015, *Acta Astronomica Sinica*, 56, 278
- Wang, N., Manchester, R. N., & Johnston, S. 2007, *MNRAS*, 377, 1383
- Weisberg, J. M., Cordes, J. M., Lundgren, S. C., et al. 1999, *ApJS*, 121, 171
- Weltevrede, P., & Johnston, S. 2008, *MNRAS*, 391, 1210
- Weltevrede, P., Wright, G. A. E., & Stappers, B. W. 2007, *A&A*, 467, 1163
- Wen, Z. G., Wang, N., Yan, W. M., et al. 2016, *Ap&SS*, 361, 261
- Wright, G. A., & Fowler, L. A. 1981, *A&A*, 101, 356
- Xilouris, K. M., Kramer, M., Jessner, A., Wielebinski, R., & Timofeev, M. 1996, *A&A*, 309, 481
- Yan, Z., Shen, Z.-Q., Wu, X.-J., et al. 2015, *ApJ*, 814, 5
- Yan, Z., Shen, Z.-Q., Manchester, R. N., et al. 2018a, *ApJ*, 856, 55
- Yan, Z., Shen, Z.-Q., Wu, Y.-J., et al. 2018b, *Radio Science Bulletin*, 366, 10
- Zhao, R.-S., Wu, X.-J., Yan, Z., et al. 2017, *ApJ*, 845, 156



**Table 1.** Parameters for the 71 pulsars observed with the TMRT

PSR J2000	MJD	Freq	$T_{\text{on}}$	$S \pm \sigma_b$	$\Delta\phi(N)$	$W_{50}$	$W_{10}$	$S^\ddagger$
Name	(d)	(MHz)	(min)	(mJy)	(deg)	(deg)	(deg)	(mJy)
J0147+5922	57721 <sup>†</sup>	4820.0	40	$2.49 \pm 0.13^*$	6.7(3)	2.9	4.1	
	57245	4920.0	30	$0.91 \pm 0.03$	6.0(3)	2.2	4.3	
				$1.70 \pm 0.80$	$6.3 \pm 0.4$	$2.5 \pm 0.3$	$4.2 \pm 0.1$	$0.35 \pm 0.11^1$
J0248+6021	57845 <sup>†</sup>	4820.0	17	$3.10 \pm 0.21^*$	–	$7.6 \pm 0.2$	$23.2 \pm 1.0$	
J0332+5434	57721 <sup>†</sup>	4820.0	30	$7.13 \pm 0.03^*$	20.2(3)	4.4	22.4	
	57378	4820.0	8	$3.37 \pm 0.07$	20.1(3)	4.5	22.6	
	57414	4820.0	8	$13.41 \pm 0.07$	20.2(3)	4.5	22.5	
	57443	4820.0	8	$14.06 \pm 0.08$	20.3(3)	4.3	21.7	
	57466	4820.0	8	$19.15 \pm 0.08$	20.1(3)	4.6	22.6	
	57536	4820.0	8	$11.47 \pm 0.07$	18.7(3)	12.3	23.0	
	57571	4820.0	8	$8.11 \pm 0.07$	20.2(3)	4.4	22.5	
	57575	4820.0	15	$7.61 \pm 0.07$	20.2(3)	4.6	22.5	
	57740	4820.0	8	$5.41 \pm 0.06$	20.4(3)	5.0	22.7	
	57760	4820.0	8	$7.03 \pm 0.07$	18.4(3)	12.5	23.7	
	57802	4820.0	8	$13.22 \pm 0.07$	20.3(3)	4.4	23.0	
	57806	4820.0	8	$6.27 \pm 0.07$	19.5(3)	4.3	21.7	
	57827	4820.0	8	$6.46 \pm 0.07$	18.5(3)	12.3	23.0	
	57844	4820.0	8	$5.11 \pm 0.42^*$	19.7(3)	4.0	22.2	
	57872	4820.0	30	$13.42 \pm 0.03^*$	20.1(3)	3.8	22.3	
	57887	4820.0	8	$18.81 \pm 0.07$	20.0(3)	3.8	22.3	
					$10.00 \pm 4.87$	$19.8 \pm 0.7$	$5.9 \pm 3.2$	$22.5 \pm 0.5$
J0358+5413	57378	4820.0	8	$6.23 \pm 0.07$	14.4(3)	5.1	25.5	
	57443	4820.0	15	$6.86 \pm 0.05$	17.3(3)	5.5	27.9	
	57536	4820.0	15	$5.89 \pm 0.05$	18.8(3)	5.1	25.8	
	57549 <sup>†</sup>	4820.0	15	$7.76 \pm 0.05$	17.8(3)	5.9	28.7	
	57576	4820.0	20	$11.38 \pm 0.04$	14.8(3)	8.8	31.7	
	57771	4820.0	15	$6.73 \pm 0.05$	15.7(3)	6.1	28.8	
	57887	4820.0	10	$5.67 \pm 0.06$	18.2(3)	7.5	30.5	
				$7.22 \pm 1.97$	$16.7 \pm 1.7$	$6.3 \pm 1.4$	$28.4 \pm 2.3$	$9.10^2, 3.36^3$
J0454+5543	57414 <sup>†</sup>	4820.0	10	$1.97 \pm 0.06$	13.1(3)	18.6	30.0	
	57443	4820.0	10	$1.75 \pm 0.06$	13.9(3)	18.9	31.4	
	57466 <sup>†</sup>	4820.0	10	$1.47 \pm 0.05$	13.3(3)	18.0	28.0	
	57571	4820.0	10	$1.57 \pm 0.06$	13.8(3)	17.8	29.7	
	57802	4820.0	10	$3.24 \pm 0.09^*$	13.3(3)	18.5	28.0	
				$2.00 \pm 0.73$	$13.5 \pm 0.3$	$18.4 \pm 0.5$	$29.5 \pm 1.5$	$0.07^2, 1.78^3$
J0528+2200	57575 <sup>†</sup>	4820.0	60	$0.27 \pm 0.02$	11.3(2)	12.9	15.4	
	57845	4820.0	30	$0.26 \pm 0.12^*$	11.1(2)	12.5	16.3	
	57887	4820.0	30	$0.30 \pm 0.03$	11.4(2)	13.2	16.5	
				$0.28 \pm 0.13$	$11.3 \pm 0.2$	$12.9 \pm 0.4$	$16.1 \pm 0.6$	$0.46^2, 0.10^3$
J0538+2817	58102 <sup>†</sup>	4820.0	24	$0.90 \pm 0.18^*$	10.8(2)	$20.9 \pm 1.4$	$37.2 \pm 2.2$	
	58114 <sup>†</sup>	4820.0	60	$0.42 \pm 0.09^*$	12.5(2)	$18.2 \pm 1.0$	$28.1 \pm 2.4$	
				$0.67 \pm 0.31$	$11.7 \pm 0.8$	$19.5 \pm 2.2$	$32.7 \pm 5.6$	
J0543+2329	57536	4820.0	30	$1.83 \pm 0.03$	–	10.8	25.9	

*Table 1 continued on next page*

Table 1 (continued)

PSR J2000	MJD	Freq	T <sub>on</sub>	S ± σ <sub>b</sub>	Δφ(N)	W <sub>50</sub>	W <sub>10</sub>	S <sup>‡</sup>
Name	(d)	(MHz)	(min)	(mJy)	(deg)	(deg)	(deg)	(mJy)
	57579	4820.0	30	1.67 ± 0.03	–	12.8	25.8	
	57845 <sup>†</sup>	4820.0	30	1.96 ± 0.16*	–	11.0	26.3	
				1.82 ± 0.22	–	11.5 ± 1.1	26.0 ± 0.3	2.79 <sup>2</sup> , 2.19 <sup>3</sup>
J0738–4042	57845 <sup>†</sup>	4820.0	15	8.06 ± 0.66*	11.3(3)	16.1 ± 0.3	30.1 ± 0.9	
J0742–2822	57291	4820.0	10	1.16 ± 0.06	5.6(2)	11.0	17.3	
	57349	4820.0	20	0.59 ± 0.04	6.2(2)	9.5	16.9	
	57378	4820.0	10	3.11 ± 0.06	5.5(2)	8.4	17.6	
	57414	4820.0	10	2.50 ± 0.06	4.8(2)	10.2	18.4	
	57466	4820.0	10	3.36 ± 0.06	5.6(2)	9.0	16.3	
	57536	4820.0	10	1.64 ± 0.06	5.1(2)	8.4	17.5	
	57549	4820.0	30	3.88 ± 0.04	4.8(2)	8.6	17.5	
	57550	4820.0	40	3.50 ± 0.03	5.3(2)	8.8	17.4	
	57571	4820.0	10	2.48 ± 0.06	5.7(2)	8.8	17.0	
	57572	4820.0	10	2.68 ± 0.06	5.6(2)	8.8	19.4	
	57579	4820.0	10	2.62 ± 0.06	5.5(2)	9.1	19.7	
	57740	4820.0	20	3.36 ± 0.04	5.4(2)	8.4	17.3	
	57760	4820.0	20	5.78 ± 0.04	5.5(2)	9.7	17.3	
	57845	4820.0	15	1.65 ± 0.13*	5.3(2)	10.8	20.0	
	57872 <sup>†</sup>	4820.0	10	2.07 ± 0.30*	5.9(2)	8.7	16.9	
	57887	4820.0	15	1.95 ± 0.05	4.7(2)	11.4	20.3	
				2.65 ± 1.29	5.4 ± 0.4	9.4 ± 1.0	17.9 ± 1.2	1.73 <sup>2</sup> , 2.47 <sup>3</sup>
J0820–1350	57350	4820.0	30	0.23 ± 0.04	2.7(2)	5.0	9.1	
	57806 <sup>†</sup>	4820.0	30	0.74 ± 0.03	2.8(2)	6.1	10.1	
	57845	4820.0	30	0.41 ± 0.04	2.2(2)	5.6	10.3	
				0.47 ± 0.27	2.6 ± 0.3	5.6 ± 0.6	9.8 ± 0.6	0.33 ± 0.03
J0826+2637	57350	4820.0	80	0.41 ± 0.02	–	3.0	6.5	
	57802	4820.0	30	0.59 ± 0.03*	–	2.7	5.5	
	57806	4820.0	30	1.62 ± 0.03	–	2.7	6.4	
	57825	4820.0	30	0.95 ± 0.03	–	2.7	6.3	
	57887 <sup>†</sup>	4820.0	30	2.21 ± 0.04	–	2.8	6.0	
				1.15 ± 0.75	–	2.8 ± 0.1	6.1 ± 0.4	0.71 <sup>2</sup> , 2.63 <sup>3</sup>
J0835–4510	57291	4820.0	8	28.61 ± 0.11	6.9(3)	13.4	23.4	
	57349	4820.0	8	24.61 ± 0.11	6.5(3)	13.3	22.5	
	57378	4820.0	8	116.15 ± 0.11	7.1(3)	13.8	23.1	
	57414	4820.0	8	79.42 ± 0.11	6.8(3)	14.3	27.4	
	57443	4820.0	8	93.93 ± 0.11	6.6(3)	13.5	22.7	
	57466 <sup>†</sup>	4820.0	8	95.42 ± 0.11	7.0(3)	13.6	23.2	
				73.02 ± 37.83	6.8 ± 0.2	13.7 ± 0.4	23.7 ± 1.8	
J0837–4135	57414	4820.0	10	2.73 ± 0.09	10.7(3)	3.7	12.8	
	57443	4820.0	10	2.30 ± 0.09	10.5(3)	3.0	12.6	
	57466	4820.0	10	2.80 ± 0.09	10.6(3)	3.1	12.5	
	57571 <sup>†</sup>	4820.0	10	6.55 ± 0.09	10.7(3)	3.0	13.1	
	57760	4820.0	10	3.46 ± 0.09	10.5(3)	3.2	12.6	
				3.57 ± 1.73	10.6 ± 0.1	3.2 ± 0.3	12.7 ± 0.2	
J0953+0755	57771 <sup>†</sup>	4820.0	110	12.76 ± 2.55	–	11.8 ± 0.1	30.1 ± 0.4	5.27 <sup>2</sup> , 41.3 <sup>3</sup>
J0953+0755i	57771	4820.0	110	0.35 ± 0.07	–	13.5	–	

Table 1 continued on next page

Table 1 (continued)

PSR J2000	MJD	Freq	T <sub>on</sub>	S ± σ <sub>b</sub>	Δφ(N)	W <sub>50</sub>	W <sub>10</sub>	S <sup>†</sup>
Name	(d)	(MHz)	(min)	(mJy)	(deg)	(deg)	(deg)	(mJy)
J1012+5307	57549 <sup>†</sup>	4820.0	140	0.17 ± 0.04	–	14.5 ± 1.8	–	0.2 ± 0.1 <sup>4</sup>
J1012+5307i	57549	4820.0	140	0.05 ± 0.04	–	11.6 ± 2.4	–	
J1136+1559	57466	4820.0	8	1.44 ± 0.07	5.0(2)	1.7	7.8	
	57570	4820.0	8	1.16 ± 0.07	5.3(2)	1.4	8.3	
	57721 <sup>†</sup>	4820.0	40	2.89 ± 0.14*	5.2(2)	1.4	8.1	
	57772	4820.0	15	3.80 ± 0.05	5.0(2)	1.4	8.0	
	57844	4820.0	30	1.48 ± 0.14*	5.3(2)	1.3	8.7	
	57912	4820.0	30	2.38 ± 0.07*	4.9(2)	1.5	8.1	
				2.19 ± 1.05	5.1 ± 0.2	1.5 ± 0.1	8.2 ± 0.3	0.92 <sup>2</sup> , 4.38 <sup>3</sup>
J1239+2453	57245	4920.0	13	1.01 ± 0.05	9.1(5)	10.5	12.6	
	57721 <sup>†</sup>	4820.0	40	1.03 ± 0.07*	8.9(5)	10.5	12.9	
	57827	4820.0	30	0.54 ± 0.03	8.3(5)	10.6	13.1	
	57844	4820.0	30	0.71 ± 0.08*	8.8(5)	10.4	12.7	
				0.82 ± 0.27	8.8 ± 0.3	10.5 ± 0.1	12.8 ± 0.2	1.50 <sup>2</sup> , 0.79 <sup>3</sup>
J1509+5531	57721 <sup>†</sup>	4820.0	30	0.54 ± 0.07*	5.9(2)	8.5 ± 0.2	12.4 ± 0.7	0.39 <sup>2</sup>
J1518+4904	57844 <sup>†</sup>	4820.0	30	0.24 ± 0.04*	–	12.5	20.2	
	58114	4820.0	60	0.36 ± 0.13*	–	12.0	21.3	
				0.30 ± 0.16	–	12.3 ± 0.4	20.8 ± 0.8	0.24 ± 0.07 <sup>4</sup>
J1559–4438	57155 <sup>†</sup>	5124.0	30	1.59 ± 0.32	17.5(3)	24.3 ± 0.6	30.7 ± 1.9	
J1600–3053	57844 <sup>†</sup>	4820.0	30	0.27 ± 0.04*	12.7(2)	27.0 ± 1.4	41.6 ± 3.5	
J1643–1224	57825 <sup>†</sup>	4820.0	30	0.68 ± 0.14	28(2)	18.9 ± 2.0	56.1 ± 6.0	0.4 ± 0.2 <sup>4</sup>
J1644–4559	57155 <sup>†</sup>	5124.0	30	30.00 ± 6.00	9.6(2)	5.48 ± 0.01	10.54 ± 0.02	
J1645–0317	57331	4820.0	23	2.34 ± 0.04	10.9(3)	3.9	17.6	
	57466	4820.0	8	1.57 ± 0.06	11.5(3)	3.4	16.8	
	57536 <sup>†</sup>	4820.0	8	1.28 ± 0.07	11.4(3)	3.6	15.9	
	57844	4820.0	30	1.34 ± 0.05	11.3(3)	3.2	16.5	
				1.63 ± 0.50	11.3 ± 0.3	3.5 ± 0.3	16.7 ± 0.7	2.35 <sup>2</sup> , 1.10 <sup>3</sup>
J1651–4246	57155 <sup>†</sup>	5124.0	30	1.15 ± 0.23	35.5(2)	16.1 ± 1.0	58.0 ± 7.7	
J1703–3241	57155 <sup>†</sup>	5124.0	30	0.72 ± 0.14	7.1(3)	10.3 ± 0.7	12.8 ± 1.2	
J1705–1906	57155 <sup>†</sup>	5124.0	30	2.43 ± 0.50	4.7(2)	10.7 ± 1.7	15.2 ± 1.9	1.10 ± 0.11 <sup>1</sup>
J1705–1906i	57155	5124.0	30	0.25 ± 0.05	–	6.0 ± 1.0	12.0 ± 1.3	0.14 ± 0.11 <sup>1</sup>
J1705–3423	57245 <sup>†</sup>	4920.0	30	1.01 ± 0.20	8.5(2)	13.7 ± 0.8	25.4 ± 2.0	
J1707–4053	57155 <sup>†</sup>	5124.0	30	0.55 ± 0.11	–	11.0 ± 1.2	16.1 ± 2.9	
J1709–4429	57155 <sup>†</sup>	5124.0	30	3.51 ± 0.70	–	19.4 ± 0.8	35.2 ± 2.4	
J1713+0747	57379 <sup>†</sup>	4820.0	10	1.42 ± 0.06	74.6(4)	9.8	82.2	
	57570	4820.0	15	1.97 ± 0.03	76.6(4)	10.1	88.3	
	57721	4820.0	26	0.52 ± 0.03*	75.8(4)	10.9	87.9	
	57772	4820.0	26	2.03 ± 0.04	73.0(4)	10.5	83.5	
	57844	4820.0	15	1.19 ± 0.11*	77.0(4)	10.5	79.3	
				1.42 ± 0.64	75.4 ± 1.6	10.4 ± 0.4	84.2 ± 3.8	0.80 ± 0.04 <sup>1</sup> , 0.8 ± 0.2 <sup>4</sup>
J1721–3532	57157 <sup>†</sup>	5124.0	30	6.03 ± 1.20	–	10.5 ± 0.2	19.9 ± 0.2	
	57844	4820.0	9	12.25 ± 1.34*	–	11.6 ± 0.5	23.2 ± 1.6	
				9.14 ± 3.59	–	11.1 ± 0.8	21.5 ± 2.3	
J1730–3350	57245 <sup>†</sup>	4920.0	30	0.83 ± 0.17	–	10.7 ± 0.6	20.5 ± 1.4	
J1739–2903	57245 <sup>†</sup>	4920.0	30	1.22 ± 0.24	–	6.5 ± 0.2	11.4 ± 1.4	
J1739–2903i	57245	4920.0	30	0.26 ± 0.05	–	7.2 ± 0.7	15.6 ± 1.6	

Table 1 continued on next page

Table 1 (*continued*)

PSR J2000	MJD	Freq	T <sub>on</sub>	S ± σ <sub>b</sub>	Δφ(N)	W <sub>50</sub>	W <sub>10</sub>	S <sup>†</sup>
Name	(d)	(MHz)	(min)	(mJy)	(deg)	(deg)	(deg)	(mJy)
J1740–3015	57157 <sup>†</sup>	5124.0	30	2.29 ± 0.46	1.4(2)	2.92 ± 0.02	6.13 ± 0.03	
J1744–1134	57802 <sup>†</sup>	4820.0	30	0.36 ± 0.02*	–	7.9 ± 0.5	22.2 ± 2.0	0.19 ± 0.06 <sup>4</sup>
J1745–3040	57292	4820.0	10	3.91 ± 0.07	26.4(3)	9.5	24.1	
	57379	4820.0	10	2.34 ± 0.06	21.7(3)	9.8	24.4	
	57572 <sup>†</sup>	4820.0	10	2.42 ± 0.06*	24.8(3)	10.0	26.0	
	57802	4820.0	10	3.46 ± 0.06	24.4(3)	9.3	24.1	
	57844	4820.0	10	1.96 ± 0.18*	24.0(3)	9.1	23.2	
				2.82 ± 0.086	24.3 ± 1.7	9.5 ± 0.4	24.4 ± 1.0	1.63 <sup>2</sup>
J1752–2806	57292	4820.0	10	1.86 ± 0.07	5.2(2)	2.9	8.9	
	57320	4820.0	25	0.83 ± 0.05	5.1(2)	2.9	8.1	
	57379 <sup>†</sup>	4820.0	10	1.58 ± 0.07*	5.9(2)	2.8	9.1	
	57444	4820.0	10	2.74 ± 0.07	4.9(2)	3.2	8.8	
	57466	4820.0	10	0.94 ± 0.07	5.5(2)	2.7	8.3	
	57570	4820.0	10	2.76 ± 0.07	5.1(2)	2.9	8.8	
	57572	4820.0	10	1.97 ± 0.07	5.5(2)	2.9	9.2	
	57844	4820.0	10	1.37 ± 0.15*	5.4(2)	2.4	8.3	
				1.76 ± 0.77	5.3 ± 0.34	2.8 ± 0.2	8.7 ± 0.4	0.44 <sup>2</sup>
J1803–2137	57245 <sup>†</sup>	4920.0	30	8.62 ± 1.72	46.3(2)	19.4 ± 0.3	88.1 ± 2.2	8.04 <sup>2</sup>
J1807–0847	57721 <sup>†</sup>	4820.0	30	1.90 ± 0.09*	16.5(3)	20.9 ± 0.3	26.5 ± 0.6	2.30 <sup>2</sup>
J1809–1917	57245 <sup>†</sup>	4920.0	30	3.56 ± 0.71	39.7(2)	57.6 ± 1.0	84.3 ± 1.8	
J1818–1422	57155 <sup>†</sup>	5124.0	30	0.79 ± 0.16	6.4(2)	4.8 ± 0.1	15.1 ± 0.4	0.51 ± 0.06 <sup>1</sup>
J1820–0427	57245 <sup>†</sup>	4920.0	15	0.57 ± 0.11	7.2(2)	3.8 ± 0.2	13.7 ± 0.9	0.43 ± 0.04 <sup>1</sup>
J1825–0935m	57415	4820.0	10	2.69 ± 0.06	13.3(2)	3.2	21.4	
	57444	4820.0	10	1.05 ± 0.06	13.6(2)	2.9	21.2	
	57467	4820.0	10	2.46 ± 0.06	11.9(2)	2.7	18.5	
	57536	4820.0	10	3.11 ± 0.06	14.3(2)	3.9	21.5	
	57570	4820.0	10	3.32 ± 0.06	13.8(2)	3.4	21.9	
	57572	4820.0	10	2.53 ± 0.06	12.8(2)	3.3	21.0	
	57721 <sup>†</sup>	4820.0	20	1.59 ± 0.05*	13.3(2)	3.3	21.4	
	57913	4820.0	30	1.20 ± 0.05*	14.1(2)	3.8	21.4	
				2.24 ± 0.88	13.4 ± 0.8	3.3 ± 0.5	21.0 ± 1.1	6.52 <sup>2</sup> , 4.76 <sup>3</sup>
J1825–0935i	57467	4820.0	10	0.32 ± 0.06	–	2.1	–	
	57572	4820.0	10	0.15 ± 0.06	–	4.2	–	
				0.23 ± 0.15	–	3.2 ± 1.5	–	
J1826–1334	57245 <sup>†</sup>	4920.0	30	4.59 ± 0.92	57.9(2)	14.2 ± 0.3	96.9 ± 1.9	2.60 ± 0.26 <sup>1</sup>
J1829–1751	57155 <sup>†</sup>	5124.0	30	1.63 ± 0.33	12.0(2)	2.45 ± 0.03	16.9 ± 0.1	1.23 <sup>2</sup>
J1830–1059	57245 <sup>†</sup>	4920.0	30	0.56 ± 0.11	–	3.8 ± 0.1	7.6 ± 0.2	
J1833–0827	57245 <sup>†</sup>	4920.0	30	2.02 ± 0.40	43.7(3)	54.6 ± 2.5	71.7 ± 4.8	0.90 ± 0.08 <sup>1</sup>
J1835–1106	57245 <sup>†</sup>	4920.0	30	0.38 ± 0.08	8.5(3)	6.9 ± 0.4	16.5 ± 1.8	
J1844+00	57155 <sup>†</sup>	5124.0	30	0.40 ± 0.03	17.7(2)	20.6	32.7	
	58090 <sup>†</sup>	4820.0	50	0.46 ± 0.03	18.2(2)	20.1	37.2	
				0.43 ± 0.05	17.9 ± 0.4	20.4 ± 0.4	35.0 ± 3.2	
J1848–0123	57155 <sup>†</sup>	5124.0	30	1.24 ± 0.25	12.8(2)	16.7 ± 0.2	23.4 ± 0.5	1.07 <sup>2</sup>
J1853+0545	57245 <sup>†</sup>	4920.0	30	0.97 ± 0.19	7.3(2)	3.2 ± 0.1	13.9 ± 0.4	
J1900–2600	57570 <sup>†</sup>	4820.0	10	1.03 ± 0.07	23.6(3)	27.8	37.3	
	57536 <sup>†</sup>	4820.0	10	0.86 ± 0.07	25.0(3)	29.4	39.9	

Table 1 continued on next page

Table 1 (continued)

PSR J2000	MJD	Freq	T <sub>on</sub>	S ± σ <sub>b</sub>	Δφ(N)	W <sub>50</sub>	W <sub>10</sub>	S <sup>†</sup>
Name	(d)	(MHz)	(min)	(mJy)	(deg)	(deg)	(deg)	(mJy)
	57292 <sup>†</sup>	4820.0	10	0.87 ± 0.07	19.9(3)	24.1	33.5	
				0.89 ± 0.16	22.8 ± 2.6	27.1 ± 2.7	36.9 ± 3.2	0.75 <sup>2</sup>
J1909+1102	57245 <sup>†</sup>	4920.0	30	0.53 ± 0.11	7.1(2)	12.7 ± 0.5	20.7 ± 1.4	
J1932+1059	57721 <sup>†</sup>	4820.0	30	7.42 ± 0.35*	2.1(2)	7.0	15.9	
	57845	4820.0	30	9.96 ± 0.80*	2.4(2)	7.1	15.6	
	57825	4820.0	10	6.34 ± 0.05	2.4(2)	7.1	15.3	
				7.91 ± 2.06	2.3 ± 0.2	7.1 ± 0.1	15.6 ± 0.3	9.08 <sup>2</sup> , 6.8 <sup>3</sup>
J1935+1616	57292	4820.0	8	3.23 ± 0.07	13.9(3)	10.5	19.4	
	57320	4820.0	20	2.57 ± 0.05	13.8(3)	10.3	20.1	
	57414	4820.0	8	3.36 ± 0.07	13.7(3)	10.1	19.5	
	57443	4820.0	8	3.73 ± 0.09	13.5(3)	10.6	20.6	
	57466	4820.0	8	1.90 ± 0.07	13.9(3)	10.5	19.7	
	57570	4820.0	8	2.62 ± 0.07	13.6(3)	10.4	20.0	
	57825 <sup>†</sup>	4820.0	8	3.93 ± 0.07	13.6(3)	10.8	22.1	
				3.05 ± 0.74	13.7 ± 0.2	10.5 ± 0.2	20.2 ± 0.9	3.99 <sup>2</sup>
J1937+2544	57245 <sup>†</sup>	4920.0	30	3.58 ± 0.72	16.5(2)	23.2 ± 0.1	30.8 ± 0.4	
J1939+2134	57721 <sup>†</sup>	4820.0	10	0.48 ± 0.02*	–	11.6 ± 0.8	20.8 ± 1.7	1.0 ± 0.2 <sup>4</sup>
J1939+2134i	57721	4820.0	10	0.07 ± 0.02*	–	7.3 ± 4.0	16.5 ± 7.0	
J1946+1805	57245 <sup>†</sup>	4920.0	15	2.58 ± 0.52	29.7(3)	37.8 ± 1.1	45.9 ± 2.2	1.71 <sup>2</sup>
J1948+3540	57155 <sup>†</sup>	5124.0	30	0.40 ± 0.08	12.4(3)	14.6 ± 0.1	16.4 ± 0.4	0.59 <sup>2</sup> , 0.5 <sup>3</sup>
J1954+2923	57245 <sup>†</sup>	4920.0	15	1.46 ± 0.29	16.8(2)	18.1 ± 0.1	22.8 ± 0.5	0.32 <sup>2</sup>
J1955+5059	57245 <sup>†</sup>	4920.0	25	0.75 ± 0.15	–	3.4 ± 0.2	7.6 ± 0.7	0.51 <sup>2</sup>
	57721	4820.0	25	0.74 ± 0.25*	–	3.5 ± 0.5	6.2 ± 1.3	
				0.745 ± 0.292	–	3.45 ± 0.55	6.9 ± 1.6	
J2018+2839	57740	4820.0	8	1.26 ± 0.07	–	7.2	15.7	
	57466	4820.0	8	1.37 ± 0.07	–	6.8	16.2	
	57740	4820.0	8	1.48 ± 0.07	–	7.7	15.0	
	57844 <sup>†</sup>	4820.0	8	1.78 ± 0.15*	–	6.4	15.7	
				1.47 ± 0.29	–	7.0 ± 0.6	15.6 ± 0.5	0.83 ± 0.09 <sup>1</sup> , 1.44 <sup>2</sup> , 0.85 <sup>3</sup>
J2022+2854	57292	4820.0	8	1.72 ± 0.07	9.1(2)	11.6	15.0	
	57351	4820.0	8	1.23 ± 0.07	9.1(2)	11.8	15.1	
	57379	4820.0	8	3.91 ± 0.07	9.5(2)	11.5	14.4	
	57414	4820.0	8	0.85 ± 0.07	9.4(2)	11.6	15.1	
	57466	4820.0	8	1.82 ± 0.07	9.4(2)	11.6	14.4	
	57536	4820.0	8	2.78 ± 0.07	9.4(2)	11.5	14.8	
	57570	4820.0	8	1.82 ± 0.07	9.5(2)	11.7	15.3	
	57572	4820.0	8	3.86 ± 0.07	9.4(2)	12.0	15.0	
	57740	4820.0	8	1.99 ± 0.07	9.2(2)	11.5	14.6	
	57802	4820.0	8	0.86 ± 0.07	9.2(2)	11.6	14.5	
	57825	4820.0	8	0.62 ± 0.07	9.0(2)	11.6	13.9	
	57844 <sup>†</sup>	4820.0	8	1.89 ± 0.16*	9.2(2)	11.9	14.8	
				1.94 ± 1.16	9.3 ± 0.2	11.7 ± 0.2	14.7 ± 0.4	1.72 <sup>2</sup> , 1.64 <sup>3</sup>
J2022+5154	57292	4820.0	8	3.98 ± 0.07	–	7.8	15.2	
	57330	4820.0	25	6.15 ± 0.05	–	7.6	15.9	
	57414	4820.0	8	5.61 ± 0.07	–	7.9	14.9	
	57536	4820.0	8	4.16 ± 0.07	–	7.9	15.2	

Table 1 continued on next page

**Table 1** (*continued*)

PSR J2000	MJD	Freq	T <sub>on</sub>	S ± σ <sub>b</sub>	Δφ(N)	W <sub>50</sub>	W <sub>10</sub>	S <sup>†</sup>
Name	(d)	(MHz)	(min)	(mJy)	(deg)	(deg)	(deg)	(mJy)
	57572	4820.0	8	5.29 ± 0.07	–	8.4	15.3	
	57721	4820.0	30	6.61 ± 0.04	–	7.9	15.0	
	57740	4820.0	10	4.87 ± 0.06	–	8.3	15.7	
	57844 <sup>†</sup>	4820.0	10	6.84 ± 0.55*	–	7.9	15.1	
				5.44 ± 1.21	–	8.0 ± 0.3	15.3 ± 0.3	3.01 <sup>2</sup> ,9.73 <sup>3</sup>
J2145–0750	57156 <sup>†</sup>	5124.0	30	1.77 ± 0.35	–	9.2 ± 0.4	66.6 ± 3.3	0.44 ± 0.03 <sup>1</sup> ,0.4 ± 0.1 <sup>4</sup>
J2257+5909	57721 <sup>†</sup>	4820.0	30	0.45 ± 0.03*	6.1(2)	9.9 ± 0.4	16.2 ± 2.4	0.38 <sup>2</sup>
J2321+6024	57845 <sup>†</sup>	4820.0	30	2.46 ± 0.22*	11.4(2)	6.1	18.9	
	57536	4820.0	10	2.66 ± 0.06	11.3(2)	6.2	18.8	
	57572	4820.0	10	1.46 ± 0.06	11.7(2)	7.4	20.0	
				2.19 ± 0.64	11.5 ± 0.2	6.6 ± 0.7	19.2 ± 0.7	1.75 <sup>2</sup> ,0.24 <sup>3</sup>
J2330–2005	57245 <sup>†</sup>	4920.0	30	0.15 ± 0.04	3.2(2)	1.7 ± 0.1	8.0 ± 1.0	
J2354+6155	57245 <sup>†</sup>	4920.0	30	1.15 ± 0.23	1.2(2)	5.7 ± 0.1	9.1 ± 0.2	0.26 <sup>2</sup> ,0.08 <sup>3</sup>

Notes: The observational parameters for 71 pulsars were derived from our measurements. Col.(2)–(4) give the MJD, central frequency and integration time for each observation; the flux densities, separation of the outer-most profile components, pulse widths at 50% and 10% of the profile maximum are given in col.(5)–(8), and the corresponding mean values are measured for pulsars that observed several times. N in col.(6) is the number of identifiable components. Col.(9) gives previously published 5 GHz flux densities; references are: 1 Kijak et al. (1998); 2 Seiradakis et al. (1995); 3 von Hoensbroech & Xilouris (1997a); 4 Kramer et al. (1999).

\* Flux densities calibrated using the calibrators (3C48, 3C123, 3C196 or 3C295).

<sup>†</sup> MJDs corresponding to the profiles in Fig.1. For three pulsars (PSRs J0538+2817, J1844+00 and J1900–2600) two or three observations are summed to form the profile in Fig.1.

**Table 2.** Characteristic parameters:  $P$ ,  $\dot{P}$ ,  $\tau$ ,  $L_{1400}$ ,  $B_{\text{surf}}$  and  $\dot{E}$  and power-law ( $\nu^\alpha$ ) indices for flux densities of 27 pulsars.

PSR J2000 Name	$P$ (ms)	$\dot{P}$	$\tau$ (Myr)	$L_{1400}$ (mJy kpc <sup>2</sup> )	$B_{\text{surf}}$ (G)	$\dot{E}$ (ergs/s)	Freq (MHz)	$\alpha$	Ref.
J0248+6021	217.1	5.5E-14	0.0624	54.80	3.5e+12	2.1e+35	1400,5000	-1.17	24
J0837-4135	751.6	3.5E-15	3.36	36.00	1.65e+12	3.3e+32	200,400 400-8600	1.05 -1.64 ± 0.12	4,12,20,21,30,31,32,33
J1012+5307	5.3	1.7E-20	4860	1.57	3.04e+08	4.7e+33	400-5000	-2.04 ± 0.15	7,13,29
J1518+4904	40.9	2.7E-20	23900	3.69	1.07e+09	1.6e+31	400-8350	-1.56 ± 0.21	11,13,25
J1559-4438	257.1	1.0E-15	4.00	211.60	5.18e+11	2.4e+33	400-728 728-5000	0.32 ± 0.75 -2.33 ± 0.24	1,2,12,15,32
J1600-3053	3.6	9.5E-21	6000	8.10	1.87e+08	8.1e+33	400-5000	-1.24 ± 0.27	26,27
J1643-1224	4.6	1.8E-20	3970	2.63	2.96e+08	7.4e+33	200-5000	-1.78 ± 0.08	6,15,16,17,26,27,30
J1651-4246	844.1	4.8E-15	2.78	432.64	2.04e+12	3.2e+32	200-5000	-2.03 ± 0.10	3,4,12,21,28,30,32,33
J1703-3241	1211.8	6.6E-16	29.1	76.37	9.05e+11	1.5e+31	400-5000	-1.49 ± 0.18	4,5,12,21,32,33
J1705-3423	255.4	1.1E-15	3.76	60.46	5.31e+11	2.5e+33	400-5000	-1.40 ± 0.08	9,21,32,33
J1707-4053	581.0	1.9E-15	4.78	115.20	1.07e+12	3.9e+32	400,640 728-5000	0.08 -2.01 ± 0.11	3,4,21,22,28,32,33
J1709-4429	102.5	9.3E-14	0.0175	49.35	3.12e+12	3.4e+36	400-8600	-0.62 ± 0.10	3,4,14,21,22,31,32,33
J1713+0747	4.6	8.5E-21	8490	15.55	2e+08	3.5e+33	1400-8350	-2.40 ± 0.40	13,25,27
J1721-3532	280.4	2.5E-14	0.176	232.76	2.69e+12	4.5e+34	950-17000	-0.78 ± 0.13	3,4,12,21,23,32,33
J1730-3350	139.5	8.5E-14	0.0226	38.98	3.48e+12	1.2e+36	400-3100 3100-8400	-1.13 ± 0.16 -0.12 ± 0.03	3,4,5,18,21,22,32,33
J1739-2903	322.9	7.9E-15	0.649	16.94	1.61e+12	9.2e+33	400-5000	-0.88 ± 0.13	4,15,21,32,33
J1744-1134	4.1	8.9E-21	7230	0.48	1.93e+08	5.2e+33	400-5000	-1.71 ± 0.22	10,13,16,17,26,27
J1809-1917	82.7	2.6E-14	0.0513	26.73	1.47e+12	1.8e+36	1170-6500	-0.11 ± 0.26	19,32,33
J1820-0427	598.1	6.3E-15	1.5	0.55	1.97e+12	1.2e+33	200-5000	-2.15 ± 0.06	4,5,26,30,32
J1833-0827	85.3	9.2E-15	0.147	72.90	8.95e+11	5.8e+35	606-5000	-1.06 ± 0.17	5,18,21,32,33
J1835-1106	165.9	2.1E-14	0.128	21.97	1.87e+12	1.8e+35	400-5000	-1.77 ± 0.11	9,21,28,32,33
J1844+00	460.5	--	--	402.36	--	--	400,1400 1400,5000	0.50 -2.35	8,21
J1853+0545	126.4	6.1E-16	3.27	68.43	2.82e+11	1.2e+34	1278,5000	-0.83 ± 0.19	20,32,33
J1900-2600	612.2	2.0E-16	47.4	6.37	3.58e+11	3.5e+31	200-800 800-10700	-1.21 ± 0.26 -2.54 ± 0.12	4,5,12,15,18,30,32,33
J1909+1102	283.6	2.6E-15	1.7	43.78	8.76e+11	4.6e+33	100-5000	-1.89 ± 0.14	4,5,18,21,32,33
J2257+5909	368.2	5.8E-15	1.01	82.80	1.47e+12	4.5e+33	100-600 600-5000	0.30 ± 0.13 -2.24 ± 0.25	5,18
J2330-2005	1643.6	4.6E-15	5.62	2.22	2.79e+12	4.1e+31	90-5000	-2.14 ± 0.12	4,5,12,18,32

Notes: Col.(2)–(7) give the period, period derivative, characteristic age, 1400-MHz psuedo-luminosity, surface magnetic field and spin-down luminosity of each pulsar. The frequency range of spectrum and corresponding spectral index are listed in col.(8) and (9). References for published data are given in col.(10).

References: 1 Manchester et al. (1978); 2 Fomalont et al. (1992); 3 Johnston et al. (1992); 4 Taylor et al. (1993); 5 Lorimer et al. (1995a); 6 Lorimer et al. (1995b); 7 Nicastro et al. (1995); 8 Camilo et al. (1996); 9 Manchester et al. (1996); 10 Bailes et al. (1997); 11 Sayer et al. (1997); 12 van Ommen et al. (1997); 13 Kramer et al. (1998); 14 Lyne et al. (1998); 15 Manchester et al. (1998); 16 Toscano et al. (1998); 17 Kramer et al. (1999); 18 Maron et al. (2000); 19 Morris et al. (2002); 20 Kramer et al. (2003); 21 Hobbs et al. (2004); 22 Karastergiou et al. (2005); 23 Keith et al. (2011); 24 Theureau et al. (2011); 25 Kowalińska et al. (2012); 26 Manchester et al. (2013); 27 Dai et al. (2015); 28 Han et al. (2016); 29 Levin et al. (2016); 30 Murphy et al. (2017); 31 Zhao et al. (2017); 32 Johnston & Kerr (2018); 33 Jankowski et al. (2018)

**Table 3.** The Spearman rank correlation  $R_s$  of spectral indices  $\alpha$  versus  $\log_{10}(x)$ , where  $x$  is one of the pulsar parameters  $P$ ,  $\dot{P}$ ,  $\tau$ ,  $L_{1400}$ ,  $B_{\text{surf}}$  and  $E$  for different data sets. The sample size for each data set is listed in parentheses after the name.  $R_s$  is the Spearman rank correlation coefficient, and  $p$  is the corresponding probability that the observed relationship has occurred by statistical chance.

Sample/Parameter	Spearman $R_s(p)$		
	AP (27)	NP (21)	MSP (6)
This work			
$P$	-0.29(0.18)	-0.718(0.001)	-0.26(0.62)
$\dot{P}$	0.32(0.14)	0.39(0.12)	-0.37(0.47)
$\tau$	-0.44(0.04)	-0.57(0.02)	0.14(0.79)
$L_{1400}$	0.30(0.16)	0.21(0.41)	-0.03(0.96)
$B_{\text{surf}}$	0.11(0.61)	0.02(0.95)	-0.26(0.62)
$\dot{E}$	0.623(0.002)	0.723(0.001)	0.37(0.47)
Jankowski et al. (2018)	AP (276)	NP (267)	MSP (9)
$\dot{P}$	0.25(3.8e-05)	0.28(4.9e-06)	0.05(0.9)
$\tau$	-0.35(1.9e-09)	-0.39(5.9e-11)	-0.5(0.17)
$\dot{E}$	0.44(4e-14)	0.43(1.4e-13)	0.33(0.38)
Han et al. (2016)		NP (572)	
$P$	-	-0.21	-
$\dot{P}$	-	0.13	-
$\tau$	-	-0.20	-
$B_{\text{surf}}$	-	0.03	-
$\dot{E}$	-	0.26	-
Lorimer et al. (1995a)	AP (343)	NP (323)	MSP (20)
$P$	-0.15(0.005)	-0.22(6e-5)	+0.51(0.020)
$\tau$	-0.22(6e-5)	-0.19(8e-4)	-

Note: AP: all pulsars; NP: normal pulsars; MSP: millisecond pulsars.



**Table 4.** Power-law fit parameters for spectral indices  $\alpha$  versus  $\log_{10}(x)$ .

Correlation	Slope	Intercept
$\alpha$ vs. $\log_{10}(P)$	$-0.12 \pm 0.14$	$-1.78 \pm 0.16$
$\alpha$ vs. $\log_{10}\dot{P}$	$0.04 \pm 0.06$	$-1.06 \pm 0.86$
$\alpha$ vs. $\log_{10}\tau$	$-0.12 \pm 0.07$	$-0.86 \pm 0.48$
$\alpha$ vs. $\log_{10}L_{1400}$	$0.25 \pm 0.11$	$-1.95 \pm 0.16$
$\alpha$ vs. $\log_{10}B_{\text{surf}}$	$0.04 \pm 0.08$	$-2.10 \pm 0.91$
$\alpha$ vs. $\log_{10}\dot{E}$	$0.29 \pm 0.07$	$-11.33 \pm 2.23$

**Table 5.** Power-law ( $\nu^\beta$ ) indices for component separations of seven pulsars with decreasing separation at higher frequencies.  $\sigma$  is the rms residual from the fit.

PSR Name	Freq (MHz)	$\beta$	$\sigma$ ( $^\circ$ )
J0358+5413	925–4820	$-0.26 \pm 0.01$	0.55
J0528+2200	408–4820	$-0.12 \pm 0.02$	0.28
J1509+5531	925–8600	$-0.23 \pm 0.01$	0.32
J1600–3053	730–4820	$-0.21 \pm 0.03$	1.29
J1826–1334	1369–4820	$-0.11 \pm 0.01$	0.60
J1937+2544	653–4820	$-0.11 \pm 0.02$	0.48
J2354+6155	408–4820	$-0.58 \pm 0.03$	0.43

**Table 6.** As for Table 5 for eleven pulsars with essentially no frequency dependence of component separation. The mean component separation,  $\langle\Delta\phi\rangle$ , is given in last column.

PSR Name	Freq (MHz)	$\beta$	$\sigma$ ( $^{\circ}$ )	$\langle\Delta\phi\rangle$
J0147+5922	1642–8600	$0.03 \pm 0.01$	0.43	5.9
J0454+5543	1400–8600	$0.04 \pm 0.01$	0.12	13.7
J0820–1350	653–4820	$-0.05 \pm 0.01$	0.09	3.2
J1559–4438	1382–4820	$0.001 \pm 0.001$	0.25	16.0
J1740–3015	1369–8600	$-0.070 \pm 0.001$	0.03	1.7
J1825–0935	408–4820	$-0.023 \pm 0.001$	0.17	16.4
J1833–0827	925–4820	$0.06 \pm 0.03$	1.00	46.1
J1909+1102	653–4820	$-0.021 \pm 0.002$	0.21	8.0
J2022+2854	410–4820	$-0.072 \pm 0.001$	0.23	9.8
J2257+5909	925–4820	$0.02 \pm 0.03$	0.32	5.0
J2330–2005	410–4820	$0.06 \pm 0.01$	0.09	3.0

**Table 7.** As for Table 5 for two pulsars with increasing separation at higher frequencies.

PSR Name	Freq (MHz)	$\beta$	$\sigma$ ( $^{\circ}$ )
J1946+1805	317–4820	$0.22 \pm 0.01$	0.55
J1954+2923	1330–4820	$0.10 \pm 0.02$	0.25

**Table 8.** Core widths and magnetic inclination angles for 23 pulsars.

PSR Name	P (s)	$W_{50}^{\text{core},5.0}$ (deg)	$W_{50}^{\text{cone},5.0}$ (deg)	Ref.	$W_{50}^{\text{core},1.0}$ (deg)	$\alpha_B^{5.0}$ (deg)	$\alpha_B^{8.6}$ (deg)	$\alpha_B^{1.0}$ (deg)
J0332+5459	0.7145	$3.22 \pm 0.02$	$3.8 \pm 0.1$ $6.1 \pm 0.1$ $8.5 \pm 0.4$ $2.26 \pm 0.02$	1	5.5	$57 \pm 0.6$	–	32
J0454+5543	0.3407	$4.3 \pm 0.2$	$2.7 \pm 0.2$ $4.1 \pm 0.3$ $11.9 \pm 2.2$	2	7.2	$67_{-7}^{+10}$	–	36
J0534+2200i	0.0331	$7.3 \pm 0.5$	–	3	–	90	$57_{-5}^{+6}$	–
J0738–4042	0.3749	$11.7 \pm 1.0$	$14.6 \pm 0.3$	2	14	$18.6 \pm 1.4$	–	17
J0837–4135	0.7516	$2.59 \pm 0.04$	$4.1 \pm 0.5$ $2.6 \pm 0.3$	2	3.7	90	$63 \pm 3$	50
J0944–1354	0.5703	$4.3 \pm 0.2$	–	3	4.6	$44 \pm 2$	–	45
J1509+5531	0.7397	$2.3 \pm 0.4$	$3.6 \pm 0.4$ $2.9 \pm 0.2$	2	5	90	–	35
J1644–4559	0.4551	$3.61 \pm 0.01$	$3.5 \pm 0.1$ $2.3 \pm 0.1$ $5.25 \pm 0.01$ $9.6 \pm 0.2$	2	6.7	$70.2 \pm 0.5$	$40.2 \pm 0.3$	33
J1645–0317	0.3877	$3.08 \pm 0.04$	$4.6 \pm 0.3$ $5.0 \pm 0.5$	2	4.2	90	$90_{-10}$	70
J1705–1906i	0.2990	$1.8 \pm 0.1$	–	2	4.5	90	$58_{-15}^{+23}$	85
J1739–2903m	0.3229	$5.45 \pm 0.05$	–	2	–	$47.8 \pm 0.6$	–	–
J1739–2903i	0.3229	$6.0 \pm 0.7$	–	2	–	$43_{-5}^{+7}$	–	–
J1740+1311	0.8031	$8.4 \pm 0.7$	$3.9 \pm 0.1$ $3.3 \pm 0.6$	3	4.1	$17.7 \pm 1.4$	–	42
J1748–1300	0.3941	$4.3 \pm 0.2$	$5.1 \pm 0.1$ $5.0 \pm 0.1$	3	4	$59 \pm 5$	–	77
J1807–0847	0.1637	$6.8 \pm 0.2$	$7.8 \pm 0.2$ $7.0 \pm 0.3$	2	$\sim 7$	$56 \pm 3$	$43_{-6}^{+10}$	60
J1825–0935	0.7690	$2.34 \pm 0.05$	$5.7 \pm 0.5$ $1.6 \pm 0.1$	2	2.8	90	–	86
J1829–1751	0.3071	$12.7 \pm 2.1$	$2.5 \pm 0.1$ $2.69 \pm 0.03$	2	9	$19 \pm 4$	–	29
J1833–0827	0.0853	$15.1 \pm 1.5$	$17.4 \pm 3.8$ $12.8 \pm 1.7$ $15.8 \pm 0.9$	2	–	$31 \pm 4$	–	–
1848–0123	0.6594	$8.7 \pm 0.6$	$4.2 \pm 0.1$ $5.6 \pm 0.2$	2	$\sim 5$	$19 \pm 1$	$19_{-2}^{+3}$	39
J1909+1102	0.2836	$9.4 \pm 1.1$	$4.7 \pm 0.5$	2	6.1	$27_{-3}^{+4}$	–	49
J1935+1616	0.3587	$4.6 \pm 0.1$	$3.4 \pm 0.3$ $4.8 \pm 0.2$	2	5.25	$56 \pm 3$	$48 \pm 4$	51
J1955+5059	0.5189	$3.0 \pm 0.1$	–	2	5.8	90	–	36
J2048–1616	1.9615	$3.9 \pm 0.1$	$2.3 \pm 0.1$ $1.80 \pm 0.03$	4	4.0	$25.0 \pm 0.8$	$53_{-11}^{+29}$	26

Note: Col.(2) gives the period of 24 pulsars; the corresponding core widths at 5.0 and 1.0 GHz  $W_{50}^{\text{c},5.0}$  and  $W_{50}^{\text{c},1.0}$  are listed in col.(3) and (5); col.(6)–(8) give the inclination angles estimated at 8.6, 5.0 and 1.0 GHz. Col.(4) gives the references for core widths at 5.0 GHz: 1 [Shang et al. \(2017\)](#); 2 This paper; 3 [von Hoensbroech et al. \(1998\)](#); 4 [Kijak et al. \(1998\)](#)

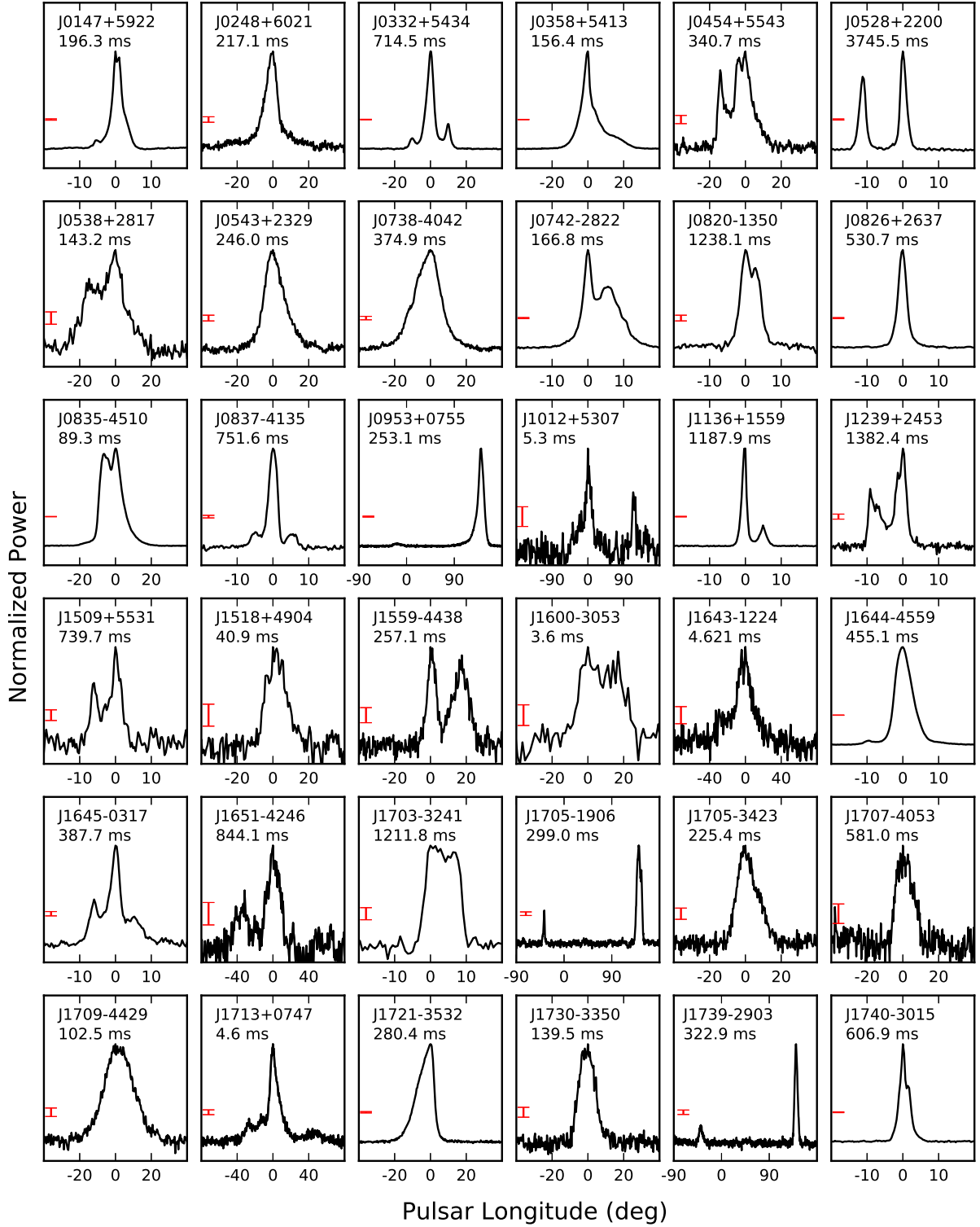


**Figure 1.** Integrated pulse profiles at 5.0 GHz obtained with the TMRT for 71 pulsars. The  $x$  axis is degrees of pulse longitude or phase and only the region around the pulse is shown. All these profiles are normalized by peak flux density, the pulse period is given for each pulsar and the red bar represents  $\pm\sigma_b$ , the rms baseline noise. Most profiles have 1024 phase bins per pulse period; six pulsars (PSRs J0538+2817, J1518+4904, J1643-1224, J1651-4246, J1703-3241, J1900-2600) have 512 phase bins per period and two (PSRs J1012+5307 and J1600-3053) have 256 phase bins per period.

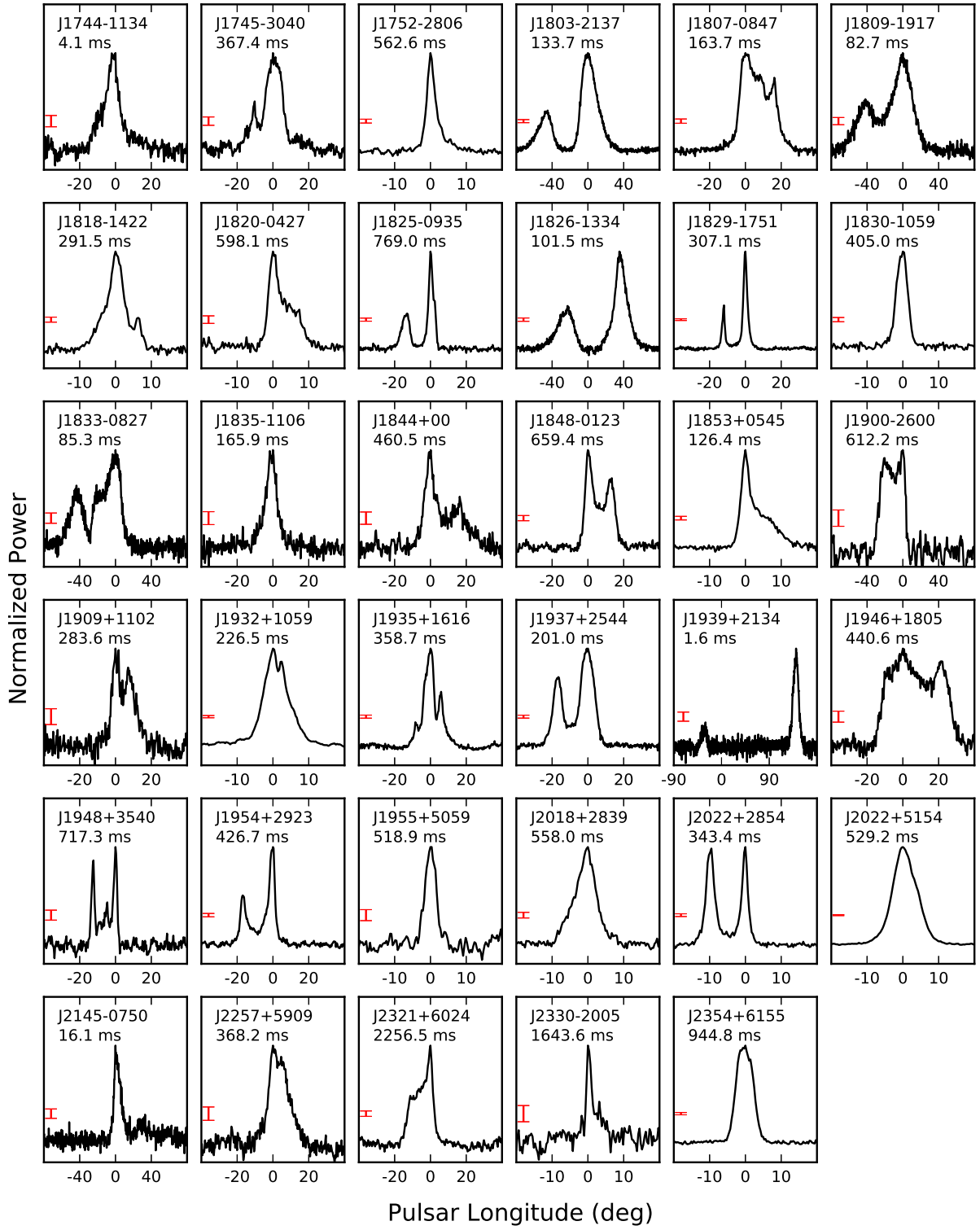
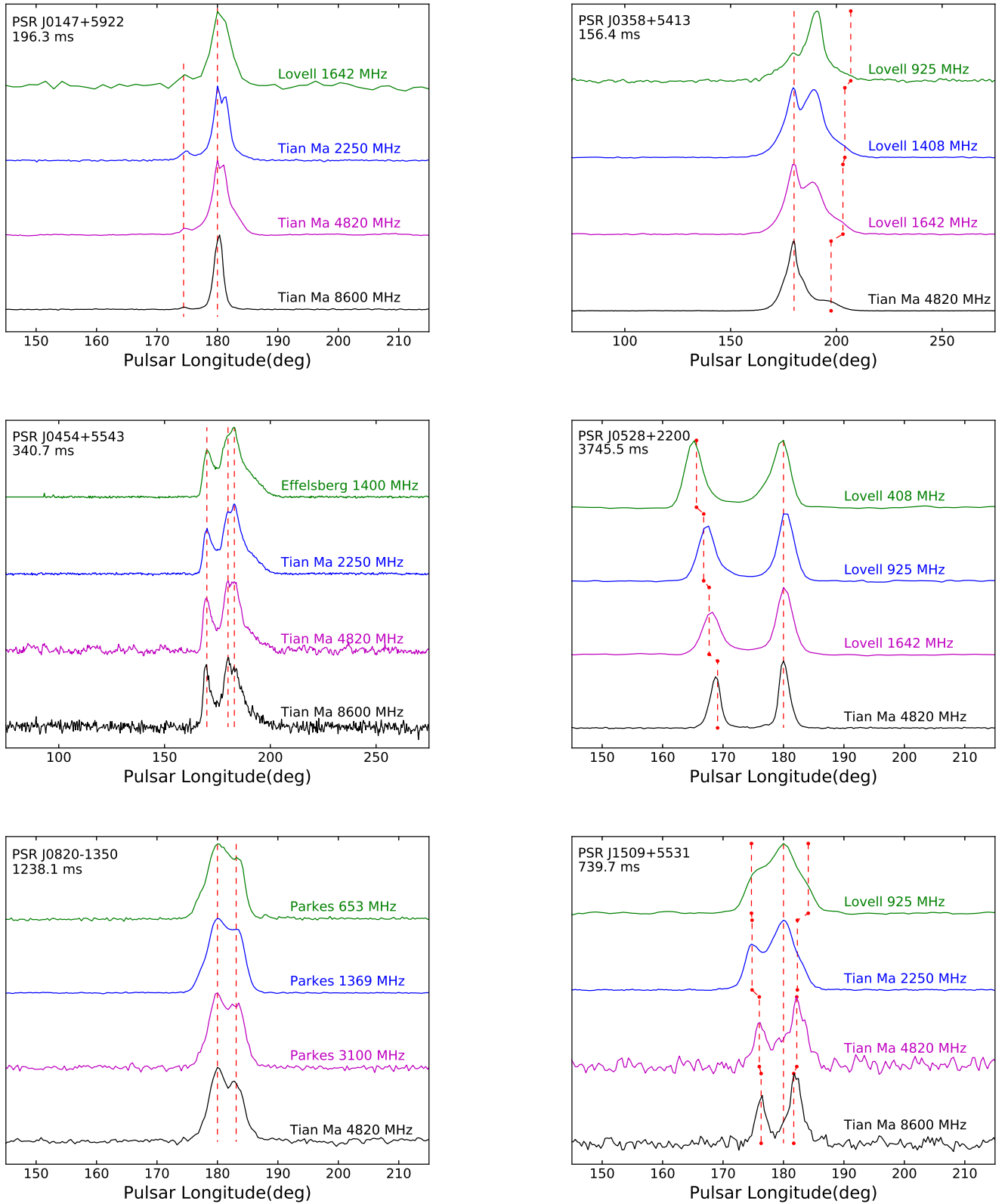


Figure 1. -continued



**Figure 2.** Integrated pulse profiles for 20 pulsars at four frequencies: 5.0 GHz from the TMRT and three other frequencies from the ATNF and EPN databases. All profiles are normalized and the corresponding components are connected by dashed lines.



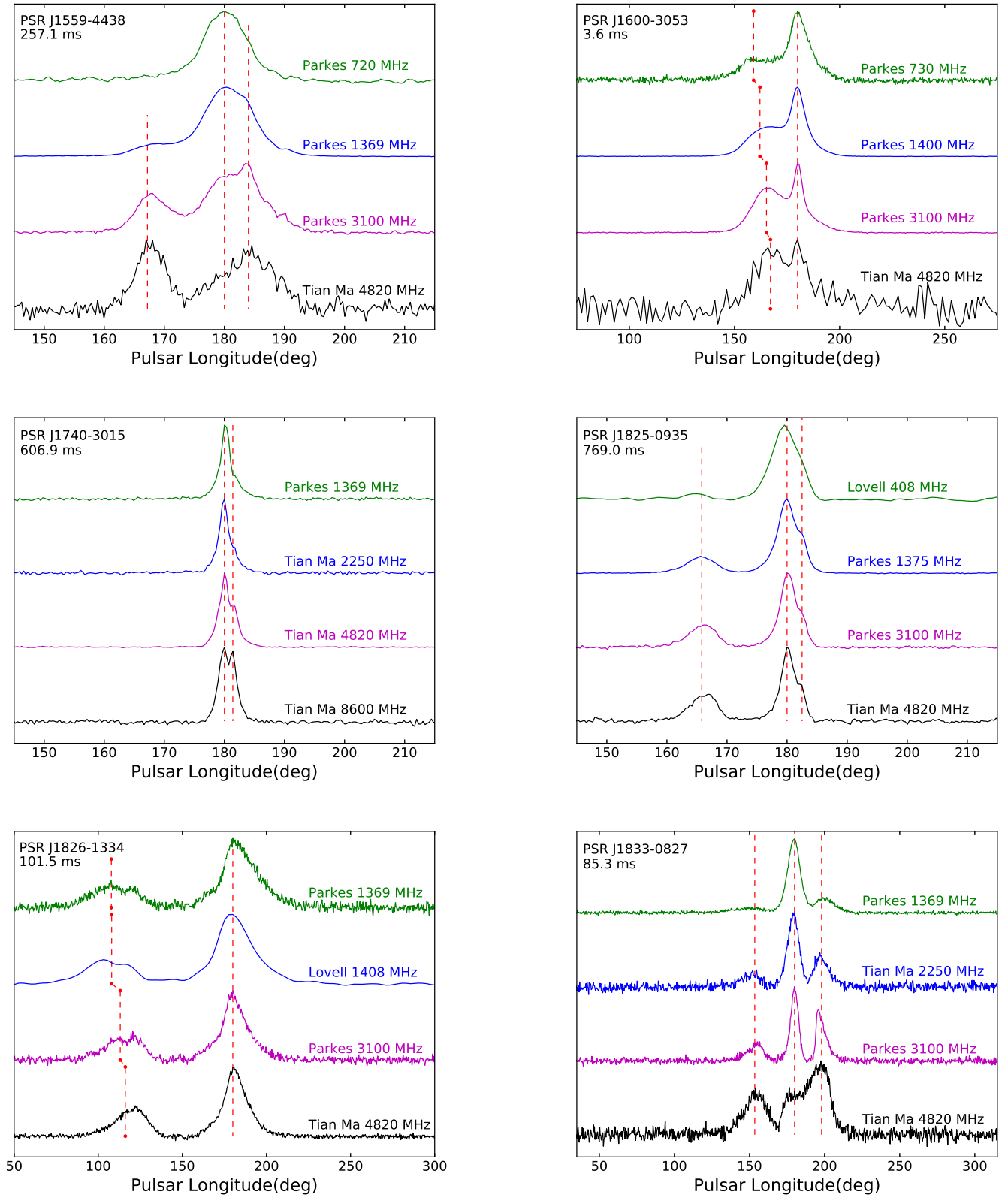


Figure 2. -continued

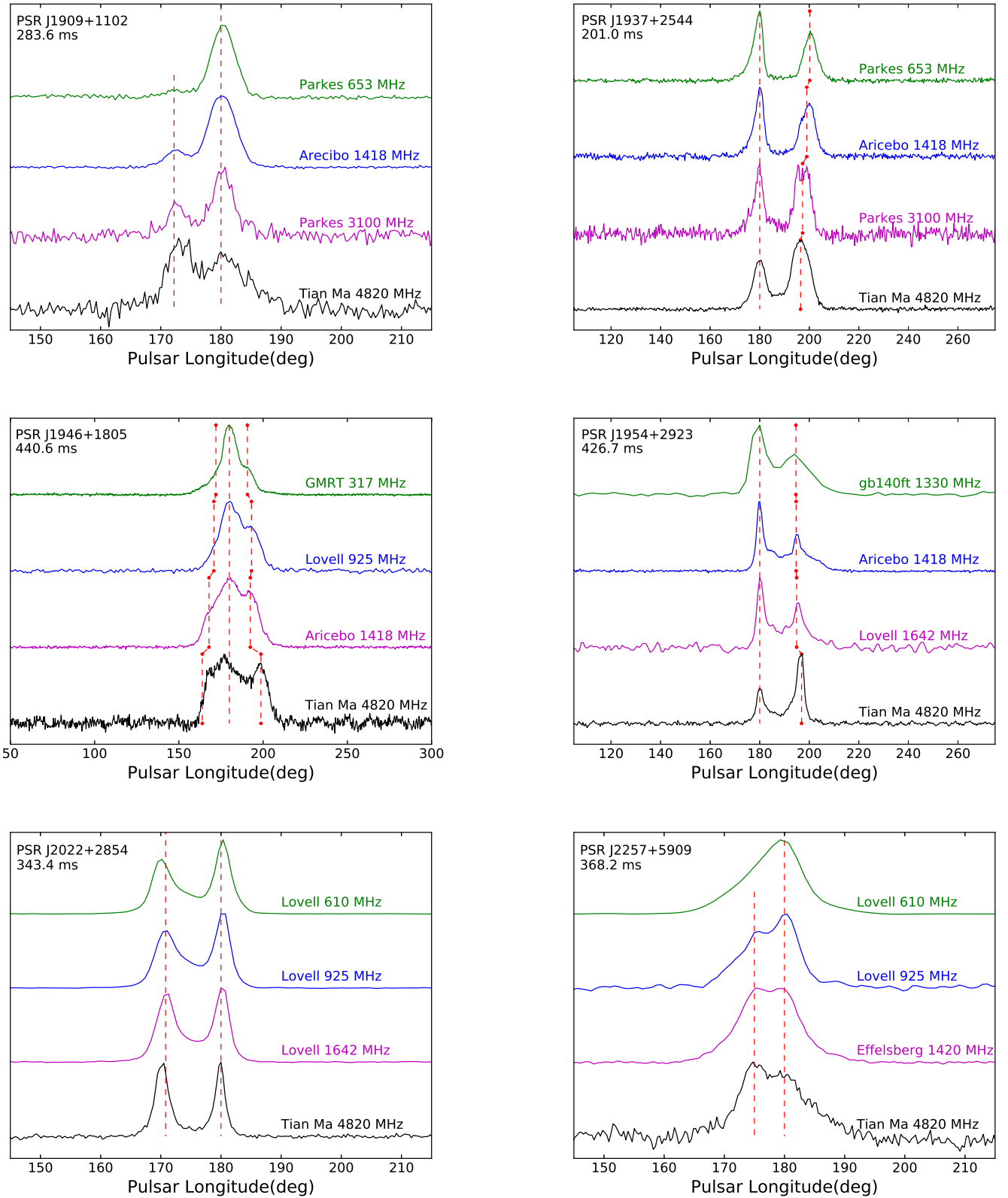


Figure 2. -continued.

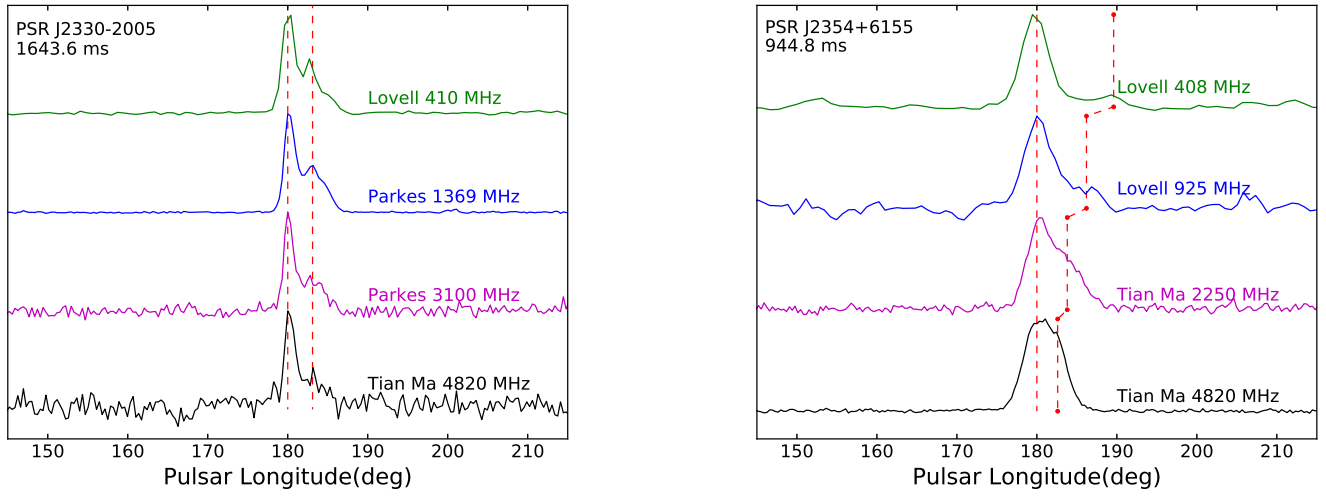
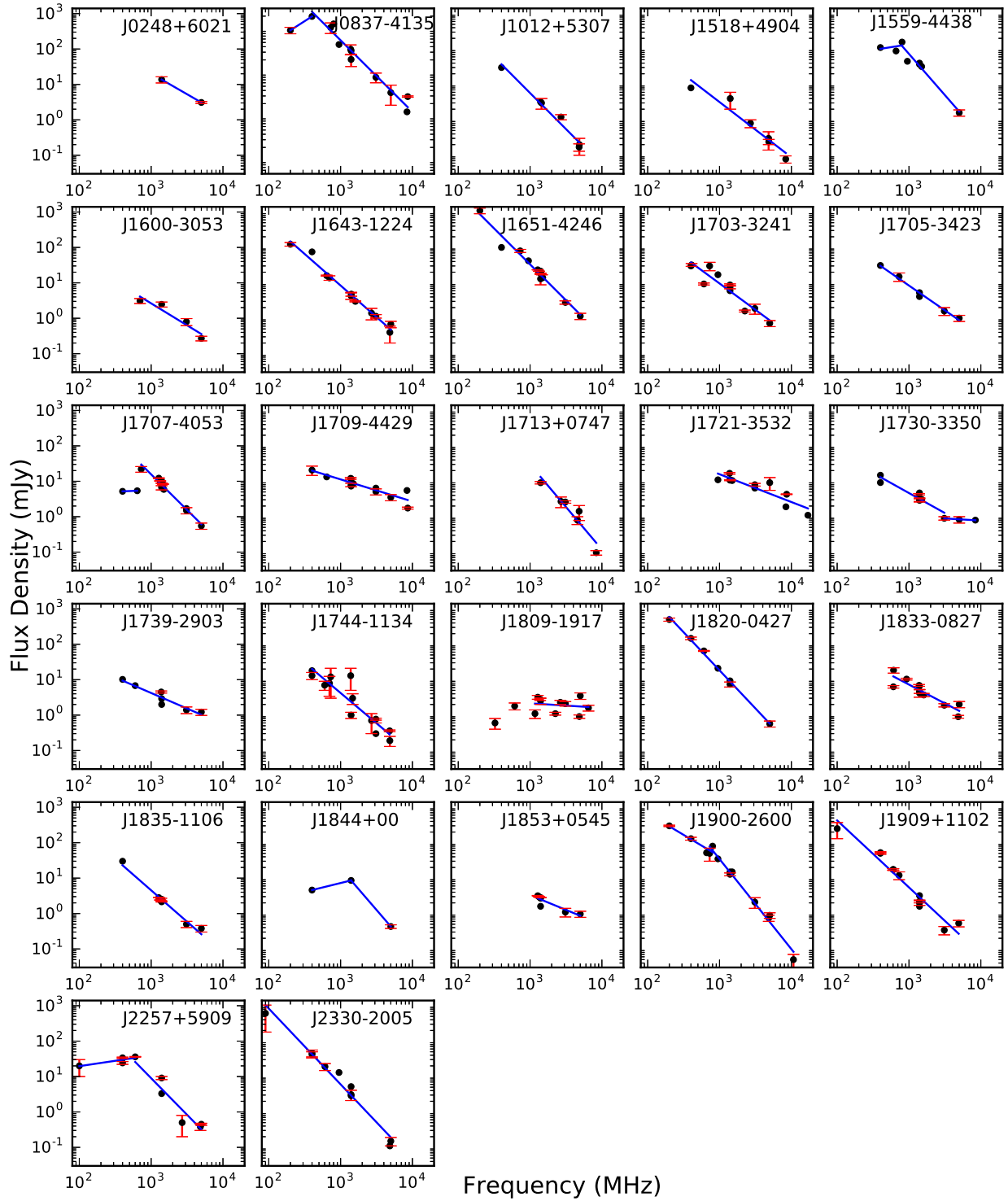
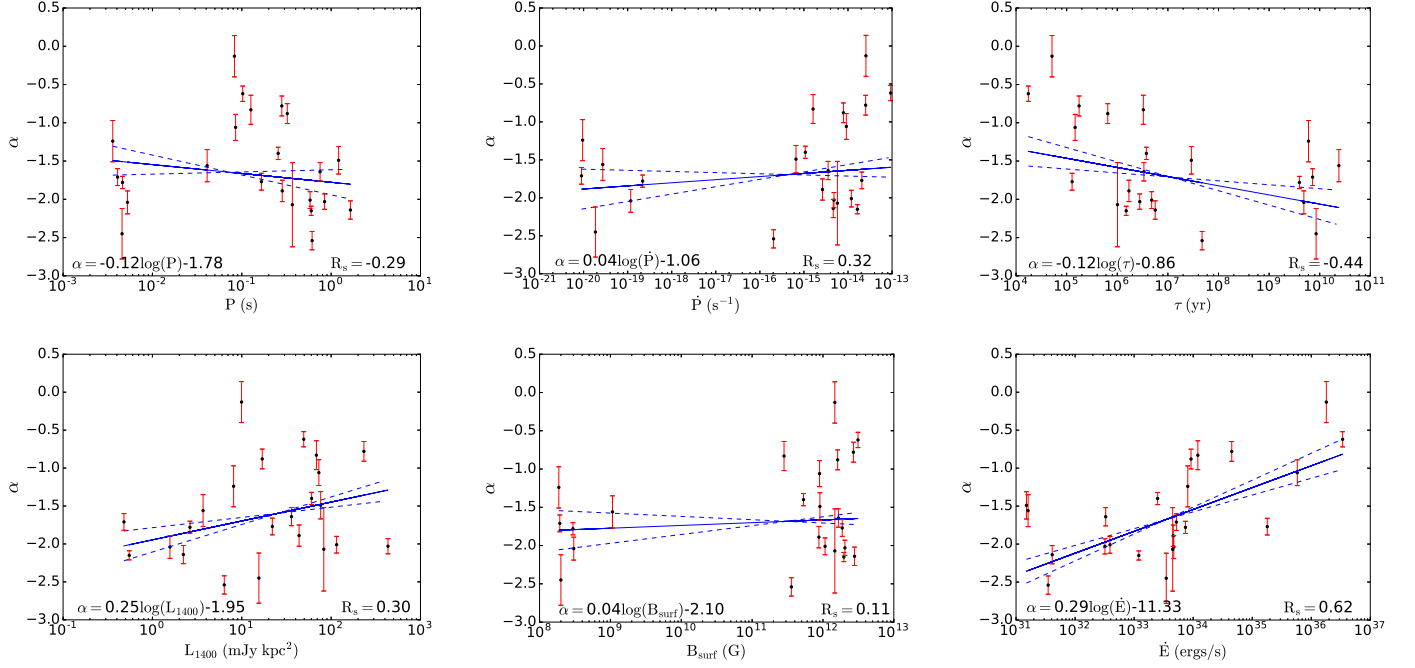


Figure 2. -continued.



**Figure 3.** Spectral plots for 27 pulsars along with power-law fits to the data. The red bars give the uncertainties of the flux densities at the different frequencies.



**Figure 4.** Distributions of spectral index  $\alpha$  versus pulsar period  $P$ , period derivative  $\dot{P}$ , characteristic age  $\tau$ , 1400-MHz pseudo-luminosity  $L_{1400}$ , surface magnetic field  $B_{\text{surf}}$  and spin-down luminosity  $\dot{E}$ . In each sub-plot, the blue line is a weighted power-law fit to the points, and the dashed lines show the  $1\text{-}\sigma$  uncertainties in the power-law index. The parameters of the fit and the Spearman rank coefficient are given at the bottom of each sub-plot.

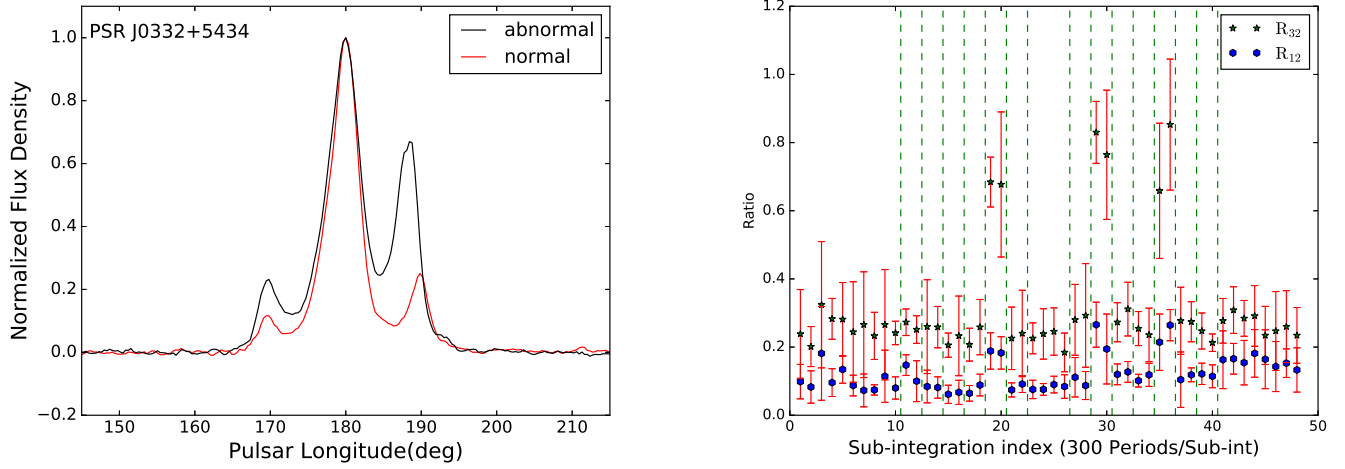


**Figure 5.** Left panel: integrated profiles for PSR J0332+5434 showing the two modes observed in TMRT observations at 5 GHz. Right panel: ratios of leading and trailing components to the central component ( $R_{12}$  and  $R_{32}$ ) for different observations separated by green dashed lines.

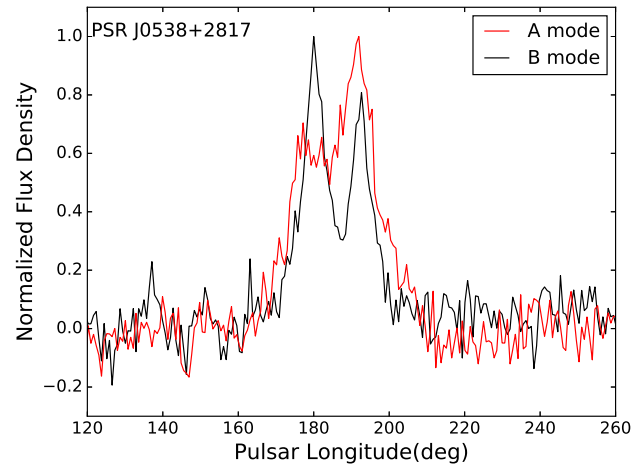


**Figure 6.** Integrated profiles for PSR J0538+2817 showing the two modes at 5 GHz obtained in TMRT observations.

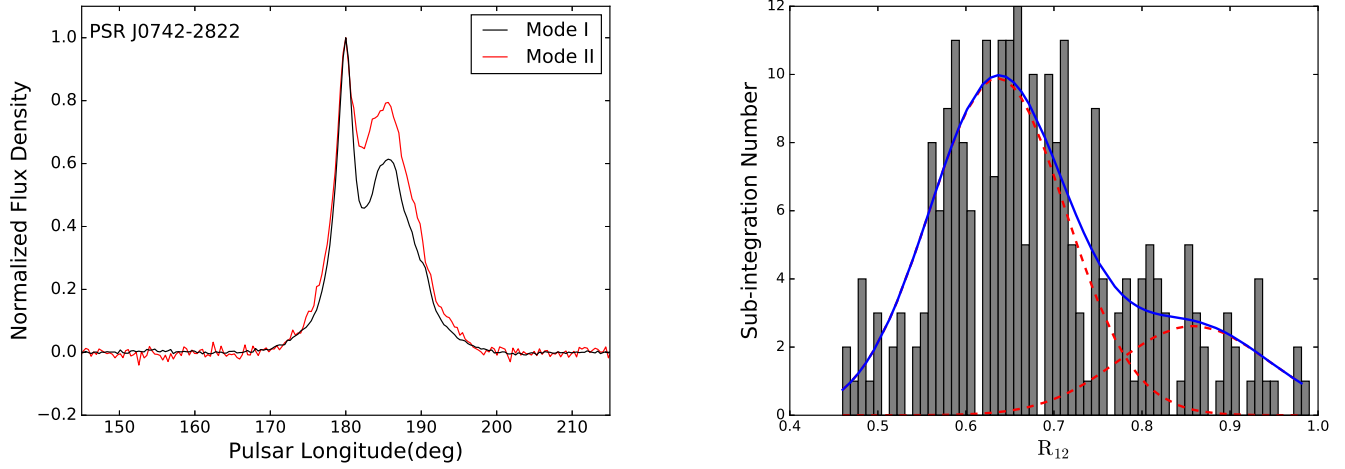


**Figure 7.** The left panel is the mode changing of integrated profile for PSR J0742-2822, whose two modes were obtained in TMRT observations. The right panel is the  $R_{12}$  distribution against sub-integration numbers. The blue line shows the fit based on two gaussian components marked by dashed lines.



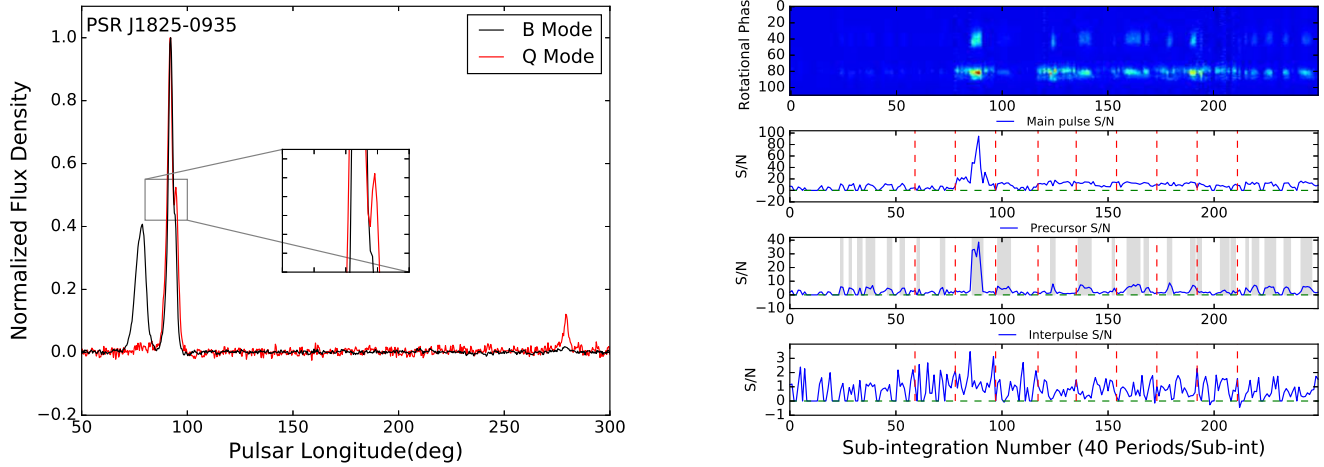


**Figure 8.** Left panel: mode changing of integrated profile for PSR J1825-0925, whose two modes were obtained in TMRT observations. Right panel from top to bottom: a zoom-in precursor and main pulse as a function of Sub-integration; the main pulse, precursor and interpulse signal-to-noise ratios of the detections in time bins of 30 s (about 40 periods). The x-axis in the bottom gives the number of 40 periods. B and Q mode were distinguished by the exhibition of precursor on/off switching (grey area). Different observations are splitted by the red dash lines.

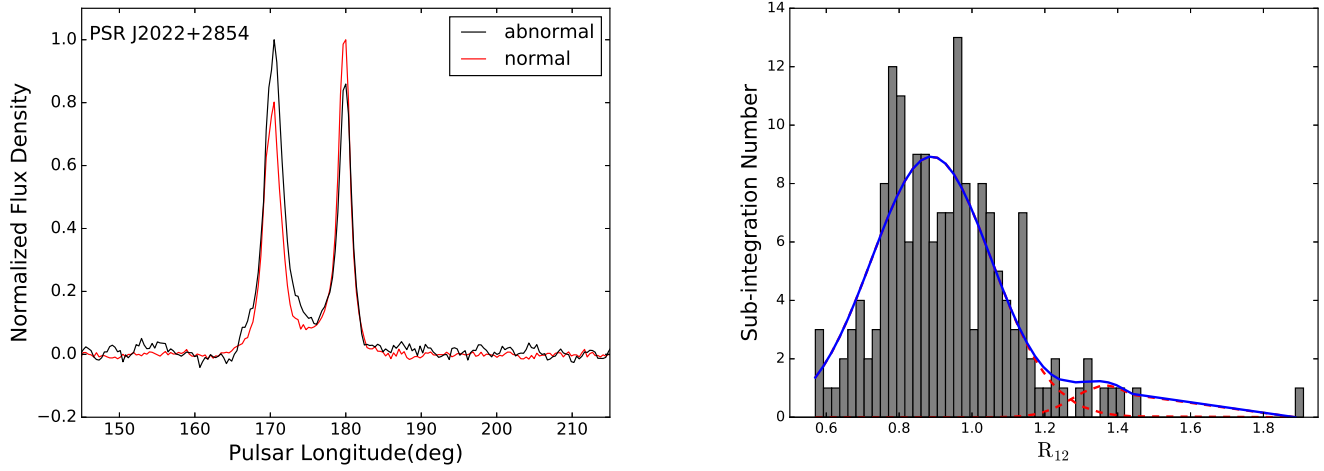


**Figure 9.** The left panel is the mode changing of integrated profile for PSR J2022+2854, whose two modes were obtained in TMRT observations. The right panel is the  $R_{12}$  distribution against sub-integration numbers. The blue line shows the fit based on two gaussian components marked by dashed lines.

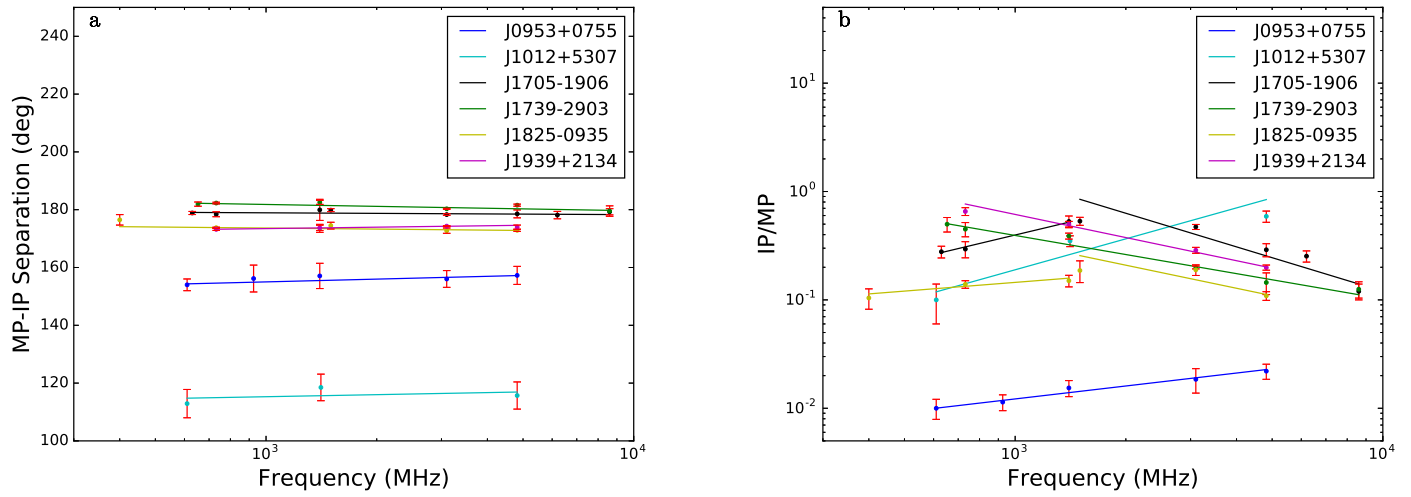


**Figure 10.** a: Separation between the main pulse (MP) and interpulse (IP) as a function of frequency for six pulsars. b: Ratio of the peak flux density of the IP to the peak flux density of the MP as a function of frequency for the same six pulsars. Weighted power-law fits to the dependencies (in some cases segmented where the over-all dependence is non-linear) are shown.

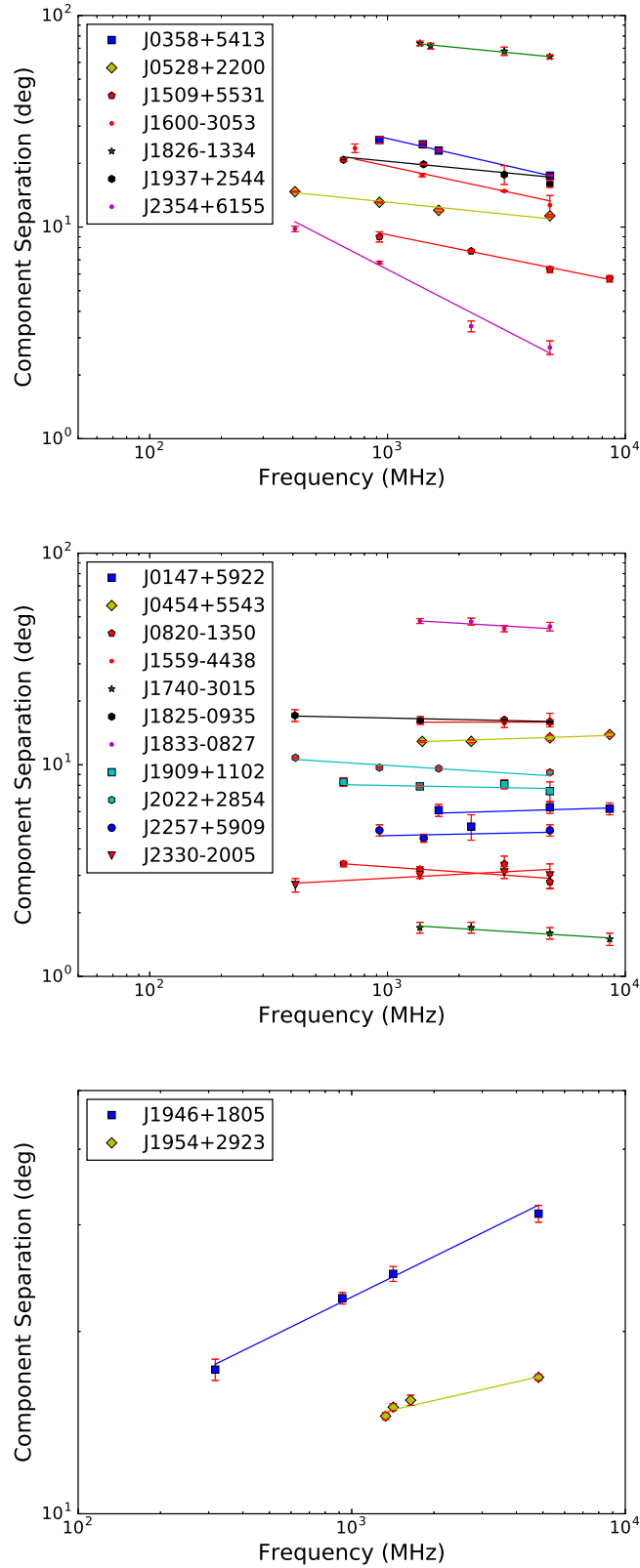


**Figure 11.** Separation of profile outermost components as a function of frequency for seven pulsars where the separation decreases with increasing frequency (upper panel), for another eleven with nearly constant component separation (central panel) and for the remaining two where the separation increases with increasing frequency (lower panel). The lines are weighted power-law fits for each pulsar.

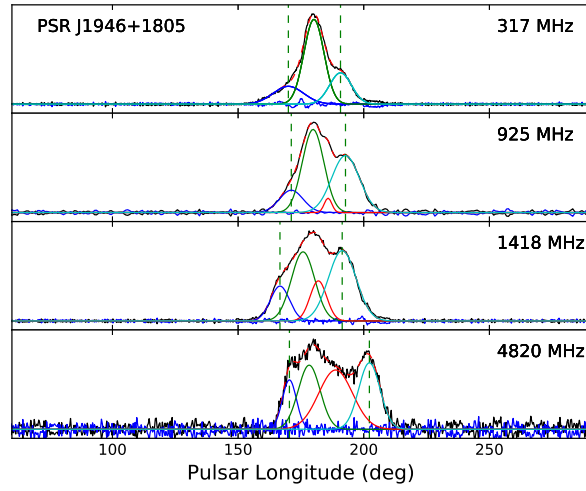


**Figure 12.** Pulse profiles for PSR J1946+1805 at several frequencies with fitted Gaussian components. Related components are identified by colour and their sum is given by the red dashed line. The fit residual is given as a blue line. The peak of outmost components are marked by green dashed line.

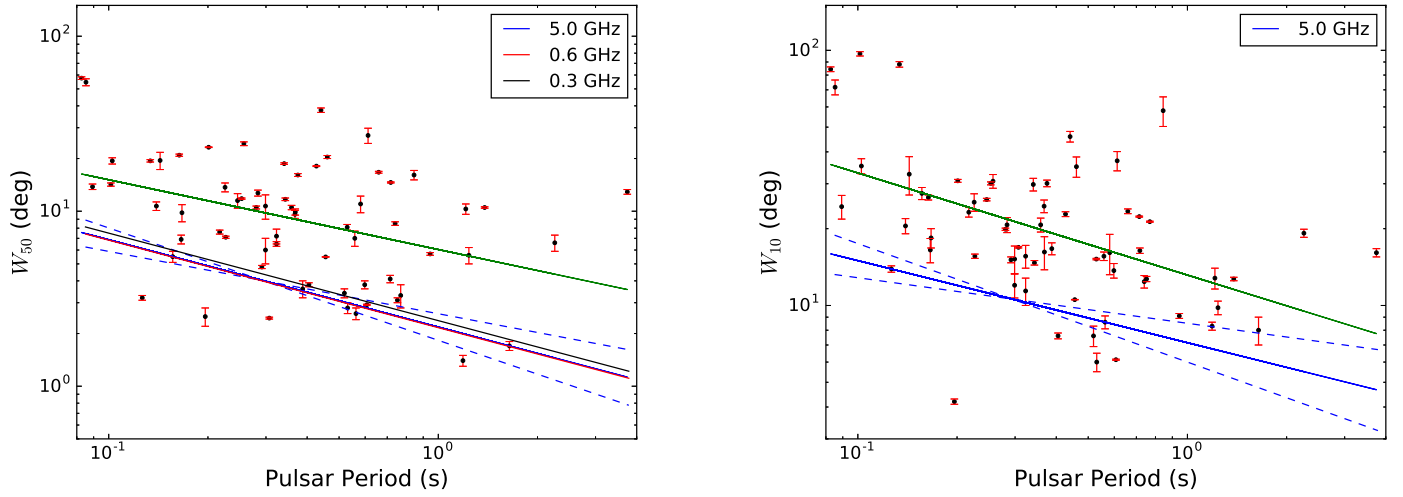


**Figure 13.** Pulse widths at 50% of the peak flux density ( $W_{50}$ ) and 10% of the peak flux density ( $W_{10}$ ) at 5 GHz for 63 pulsars. (The eight millisecond pulsars in our sample were excluded as they form a distinct class.) The green lines are power-law fits with the same slope of  $-0.37$  for  $W_{50}$  and  $W_{10}$ , respectively. The blue lines in both figures are the 5 GHz estimate of the lower boundary line using quantile regression, and the errors from our fits were marked by blue dashed lines. The red and black lines in the left panel are the lower boundaries of  $W_{50}$  at 0.6 and 0.3 GHz, respectively (Skrzypczak et al. 2018).

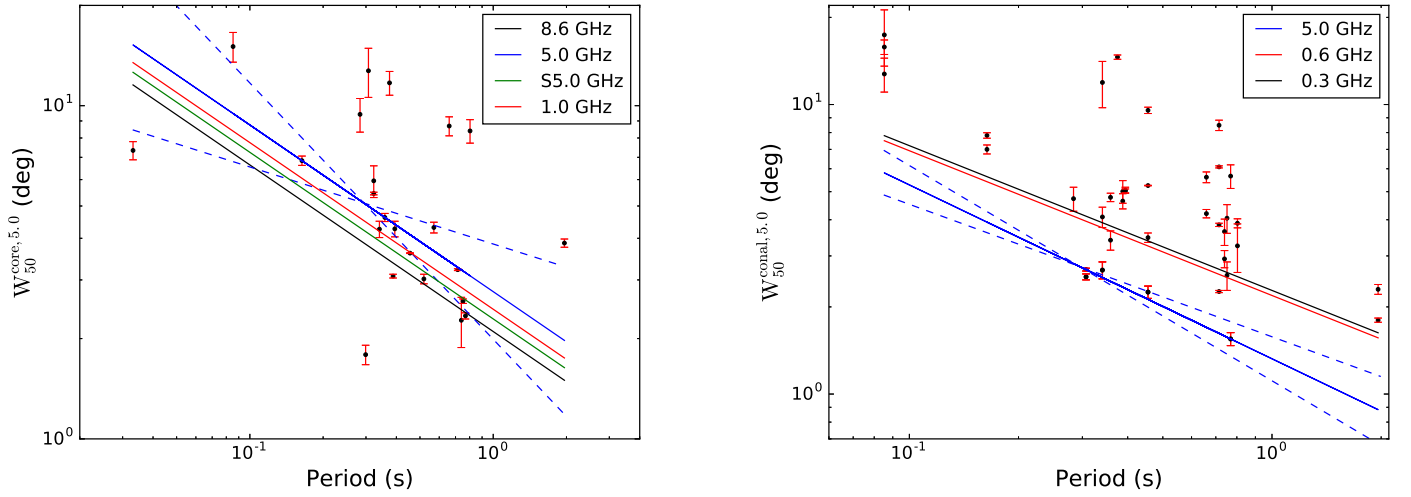


**Figure 14.** Observed core- and conal-component half-power widths at 5.0 GHz plotted against pulse period. The blue lines in both figures are the 5 GHz estimate of the lower boundary line using quantile regression, with the errors from our fits were marked by blue dashed lines. The lower-bound relations in the left panel are from Rankin (1990) from 1.0 GHz observations (red line), from Zhao et al. (2017) from 8.6 GHz observations (black line) and from the scaled Rankin (1990) fit (green line). The red and black lines in the right panel are the lower boundary of conal-component half-power widths at 0.6 and 0.3 GHz respectively from Skrzypczak et al. (2018).